Abstract

YOGANAND N SARIPALLI. Integrated AlN/Diamond heat spreaders for silicon device processing. (Under the guidance of Dr. Jag Kasichainula.)

Diamond with its very high thermal conductivity is an excellent choice for spreading heat produced during the operation of all electronic devices and in particular, high power and high frequency devices. Hitherto, diamond heat spreaders have been bonded to silicon devices using metallization and soldering layers. However, the interfacial thermal resistances at the interfaces decrease the effective thermal conductivity of the bonded heat spreader. Although direct growth of diamond on Si is expected to reduce the interfacial resistance, it has not been attempted. Contamination of the device wafers from carbon, oxygen and other impurities by diffusion during the growth of diamond could be a limiting factor. Moreover, diamond oxidizes above 600^{o}C in the presence of oxygen and may not be stable during oxidation and other high temperature steps in silicon device processing. Growth of diamond by CVD is not defect free and contains voids that decrease the thermal conductivity. Hence, a buffer layer of AlN that fills these voids and thereby reduce the thermal resistance is thought to be beneficial.

The growth and characterization of AlN and diamond films on the backside of Si (100) wafer with silicon nitride on the device side is investigated. AlN films were deposited by pulsed DC reactive magnetron sputtering at 600^{o}C. Diamond film was deposited by microwave plasma chemical vapor deposition at 900^{o}C. The films were characterized by X-ray diffraction (XRD) and transmission electron microscopy (TEM) for crystalline quality, by scanning electron microscopy (SEM) for morphology, and by infrared thermography for heat spreading characteristics. The heat spreading

characteristics of the wafer with the composite AlN/diamond films were found to be superior to that of wafers with no heat spreaders or to the wafers with either single layer diamond or single layer AlN heat spreaders. Deep level transient spectroscopy (DLTS) and secondary ion mass spectroscopy (SIMS) were performed on the samples with and without the heat spreader for determining the concentration of the impurities. The results showed that the purity of the wafers is not altered. The device characteristics were studied by fabrication of Schottky diodes on the wafers with the composite AlN/diamond heat spreader and compared with that of devices on wafers with no heat spreader. The device characteristics were found to be similar and unaffected by integration with AlN/diamond heat spreader. Thus, the integration of AlN/diamond heat spreaders with silicon device processing has been shown to be successful.

Integrated AlN/diamond heat spreaders for silicon device processing

By

Yoganand N Saripalli

A thesis submitted to the graduate faculty of
North Carolina State University
In partial fulfillment of the
Requirements for the Degree of
Master of Science

Materials Science and Engineering

Raleigh

2002

APPROVED BY:

_____	_____
Minor representative	Member

_____

Chair of advisory committee

Biography

Yoganand Saripalli was born in Kakinada, India. He studied in Visakhapatnam where he graduated from Sri Satya Sai Vidya Vihar high school in 1995. Upon graduation from high school, he enrolled at Andhra University, Visakhapatnam, India, where he pursued Bachelors degree in Metallurgical Engineering. He completed the B.E degree in May of 1999. Upon graduation from Andhra University, he attended the North Carolina State University where he pursued M.S in Materials Science and Engineering. He completed the M.S. degree in April of 2002, and completed a Masters thesis in *Integrated AlN/diamond heat spreaders for silicon device processing*. Having completed his M.S, he decided to continue his studies for a doctoral degree in Material Science and Engineering in the field of optoelectronics.

Acknowledgements

First of all, I would like to thank Dr Jag Kasichainula, my advisor, for all the encouragement while working on this project. I would like to thank him for the constant support, training, and guidance he provided me with, throughout the course of my study. I would also like to thank Dr. Ronald Scattergood and Dr. Carl Osburn for agreeing to be on my advisory committee and their helpful comments.

I would like to thank Dr. A. Karoui for his help and advice in conducting DLTS. I sincerely appreciate Dr. D.G. Yu and Ms. Joan O' Sullivan for their advice, help and guidance given during device processing in the clean room at AEMP, in EGRC. I would also like to thank Mr. Roberto Garcia and Ms. Laura Smith of AIF for training me in the use of SEM and helping me when I encountered problems. I also thank Dr Dieter Griffis for his help in conducting the SIMS analysis.

I would like to thank Dr. Hsin Wang of Oak Ridge National Laboratory for allowing me to use the facilities in HTML and his help and advice in performing infrared thermography measurements. I also thank my group member Mr. S. Makala for good discussions and support during the course of my research.

I also thank Mr K. Sagi for the accomodation provided and making my stay at Oak Ridge-Knoxville a pleasurable one. I would like to thank all the staff of Department of Materials Science and Engineering, especially Ms. Edna Deas for being so helpful during my MS program

In the end, I would like to thank my family and friends for having been a great moral support and motivation during my course of study.

This research work was supported by National Science Foundation.

Table of contents

List of Tables

List of Figures

Appendix

Integrated AlN/diamond heat spreaders for silicon device processing

Yoganand N Saripalli

Thesis advisor: Dr Jagannadham Kasichainula

Dept. of Materials Science and Engineering

North Carolina State University.

Chapter 1

Introduction

INTRODUCTION

As the present day advances in the field of ULSI technology approach the sub-micron range, it arises concern about the thermal stability and the lifetime of the devices. The devices very much depend on the metallization schemes for gates, interconnects, ohmic contacts. The reliability of these with the metals being used as current carrier that are aluminum, and more recently copper is questionable because of high current density. Integrated circuits normally operate at temperatures in the range of 25-80^{o}C. However, power devices and high power integrated circuits normally operate at temperatures as high as 300^{o}C[1]. At such higher temperatures, metallurgical reactions could easily occur, impurity redistribution may take place, and the stability and the reliability of the device is compromised. The major problems in the devices are associated with the stability of the metallization at high temperature. For example, these include thermally induced changes like grain-growth, thermal expansion and residual stresses. Changes in the resistivity, electromigration, and the reaction of the metallization with other materials in contact like dielectric layers, semiconductor, and top level metal, all contribute to the instability. Thus, heat generated during device operation can be regarded as the enemy of most micro-electronic circuits. Therefore, efficient removal of heat is essential if the circuit is to function properly[2]. These deficiencies can be solved by either choosing the materials for fabrication that could sustain the thermal instabilities, or by providing efficient built in cooling system with the device. Much research has been performed in the choice of materials, however, the thermal stability of high power devices still remains a concern. Electronic power devices such as microwave power antennas and laser diodes are susceptible to failure by the dissipation of heat generated from the active regions[3]. At this

juncture it is worth examining, and considering the use of heat spreader coatings that can efficiently spread away the heat produced during the operation of the device, and thereby increase device lifetime and reliability.

Diamond offers a unique combination of properties that make it ideally suited for electronic materials: highest thermal conductivity, high electrical resistivity, and low dielectric constant. Diamond is unmatched in its thermal conductivity. The transfer of heat in dielectric materials like diamond is based on thermal phonons, which is the directional wave motion of interacting lattice ions. This is dominant in diamond because of its strong and rigid bonded structure making it an excellent thermal conductor. Growth of diamond has been a great limitation until the CVD technique of diamond growth was discovered. With the advent of large area CVD diamond deposition, it is now possible to consider the use of diamond in electronics[2,4] for heat removal. The properties of CVD diamond are listed in Table 1.1

Electrical properties of diamond[5]:

1. Diamond can efficiently transport or transmit energy in the form of phonons, microwaves, visible and infrared radiation.
2. The bandgap of diamond is 5.5ev and corresponds to wavelength of 225nm in the electromagnetic spectrum. If diamond is polished, the defects created will induce energy levels in the bandgap and enable efficient ultraviolet absorption and emission.
3. Diamond displays exceptional charge transport properties and emits electrons at very low applied fields.
4. Diamond also possesses variable work function (high for p-type and low for intrinsic and n-type) and negative electron affinity.

These unique properties of diamond enable it to be used in electronic packaging. Diamond's high thermal conductivity allows rapid dissipation of thermal energy away from devices in electronic subsystems[2]. The CVD grown diamond can be used for the following thermal management applications[4].

1. Laser diode heat sinks: Laser diodes can be designed with a very high power density with the heat spreading capability of diamond that will significantly lower the junction temperature. The solder layer between the laser and diamond is the limiting factor and should not present an excessive thermal impedance. Laser diode arrays with very high power outputs represent another good application for diamond as heat spreader. Use of diamond heat sink for monolithic AlGaAs laser diode arrays that have power outputs exceeding 100W, was estimated to decrease the thermal resistance of the high power diode by 50%[6].
2. Microwave substrates: Microwave circuits require the dissipation of high power from small monolithic microwave integrated circuits (MMIC). Frequency divider circuits used in the avionic's automated test system for aircrafts showed improved heat dissipation when fabricated on diamond substrates rather than alumina.
3. Single chip packages: Single chip packages in future are expected to operate at 50-100W. At these high power levels, use of diamond heat sinks in place of copper-tungsten can significantly improve the reliability.
4. Power device modules: Power semiconductor devices such as MOS-controlled thyristors (MCT) and insulated gate bipolar devices (IGBT) have heat fluxes more than 200W/cm^2. Diamond is a promising candidate for reducing the thermal impedance in these devices.

5. Microelectronic packaging: Packaging of the power electronics of a flight computer, and the three-dimensional packaging of a complete digital computer system are starked by the problem of thermal management. This problem can be greatly solved by the use of diamond substrates due to its high thermal conductivity[2].
6. Aerospace applications of diamond[5]: Diamond is used in making infrared windows for hypervelocity interceptors. Diamond substrates are used for the development of multichip modules and heat spreading substrates for high-speed processors and related applications.
7. Other applications[7]: Other applications of diamond include optically triggered high powered switches in radar systems, x-ray windows, x-ray targets, artificial heart valves, scalpels, and marine fouling wherein the diamond plating of ships and underwater objects helps in the increased lifetime of the ship hulls.

It can be seen that diamond with its unmatched properties, can be used in a wide range of microelectronic applications. In the present study, the application of diamond as a heat spreader and its integration into silicon device processing is explored.

Motivation

However, continuous and defect free growth of diamond is a difficult task[7]. The presence of defects reduces the thermal conductivity diamond and it may not be an effective heat spreader. In particular, the thermal resistance of the voids is very large[8]. A high thermal conductive phase that replaces the amorphous or void like regions will be helpful in decreasing the thermal resistance. Aluminum nitride with a good thermal conductivity of 3.7W/cm-K can be used to fill the void like regions formed during growth of diamond and increase the thermal conductivity of the diamond layer. Thus, the multilayer

diamond/AlN/diamond or AlN/diamond composite structure can be used as effective heat spreader[8]. Aluminum nitride, a very good diffusion barrier for carbon, is also reported to be a buffer layer for diamond growth[9]. Apart from these advantages, aluminum nitride can be easily deposited by either reactive magnetron sputtering, or by pulsed laser deposition. Thus, the choice of aluminum nitride is clear in fabricating the multilayer heat spreader structures of diamond. Though, diamond adds to the thermal conductivity of a substrate and improves the heat spreading characteristics, the integration of diamond heat spreaders with silicon technology hasn't been attempted. The contamination that can occur in the Si wafer during diamond deposition is thought to be a probable reason [10] behind this. Because of this reason, hitherto, diamond has been bonded to the substrates like silicon using a gold-tin eutectic alloy solder film[8]. However, the thermal resistance of the multilayer heat spreader shown in Fig.1.1 increases at the interface of the metallization layers on diamond, on backside of silicon, and at the solder. Resistance at four interfaces exists with this method of bonding the silicon wafers to diamond. The interfaces that contribute to the total thermal resistances are (a) silicon/metallization, (b) metallization/solder, (c) solder/metallization and (d) metallization and diamond. The thermal resistance arising from the above interfaces and attachments strongly impedes the cooling by conduction. The interfacial resistance could be reduced in the case of direct growth of aluminum nitride and diamond on Si as shown in Fig. 1.2. Only two interfaces; Si/AlN and AlN/diamond are present, thus effectively reducing the total interfacial thermal resistance. Apart from this, the poor adhesion of diamond to the metallization layer poses another problem[8] in particular in high frequency power devices. Thus, it is thought that direct growth of diamond on the backside of the electronic substrates such as

silicon could be more effective in the spreading of heat. The direct growth of diamond on Si to measure the thermal resistance of the diamond/Si interface was experimented[12], however, with no use of the buffer AlN layer. Moreover, hitherto integrating these heat spreaders into silicon technology has not been tried. Thus, the integration of the diamond heat spreaders into silicon technology needs to be investigated.

Integration of the diamond heat spreader with silicon device wafers was investigated in the present effort. Because the diamond growth is carried out between 900-950^{o}C on the backside, contamination from the impurities present in the gas mixture is considered a drawback to be overcome. Silicon wafers coated with silicon nitride on the front side were used to prevent the contamination. Further, AlN diffusion barrier films were used to prevent the diffusion of impurities from the backside during diamond growth. AlN, with its good thermal conductivity is also thought to prevent the void formation in the initial stages of diamond growth and thus improve the effective thermal conductivity of the heat spreader. Because the integrated device wafers with AlN/diamond films on the backside are expected to undergo high temperature oxidation treatment during device processing, the stability of the wafers against impurity concentration was studied. The device integration was tested by fabrication and characterization of Schottky devices on the substrates with AlN/diamond films on the backside. The stability of the device wafers during high temperature processing was verified by high temperature oxidation treatment, and further processing and testing of Schottky devices on the wafers. The growth and orientation of the films was characterized by transmission electron microscopy and X-ray diffraction and the morphology by scanning electron microscopy. The impurity concentration that may be

introduced in the device wafer was determined by deep level transient spectroscopy (DLTS) and secondary ion mass spectroscopy (SIMS). Table 1.2 lists the samples used for the integration of the heat spreader and different characterization techniques employed to prove the successful integration of diamond heat spreaders into silicon technology.

The present study comprises the integration of the multilayer aluminum nitride/diamond heat spreaders with device processing, characterization, and testing to determine the stability of the wafers during high temperature treatment.

References

1. S.P. Murarka, Metallization, theory and practice for VLSI and ULSI. (Butterworth-Hienemann, Boston) 1993, pp 2-3.
2. L.M. Napolitano Jr, D.D. Andaleon, M.R. Daily, E. Meeks, D. Miller, D.P. Norwood, D.W. Peterson, C.A. Reber, J.E. Robles, and W. Worobey, 2nd International conference on the applications of diamond films and related materials. Editors: M. Yoshikawa, M. Murakawa, pp 275, 1993.
3. K. Jagannadham, and H. Wang, Report submitted to ORNL, 1998.
4. G. Lu, 2nd International conference on the applications of diamond films and related materials. Editors: M. Yoshikawa, M. Murakawa, pp 269, 1993.
5. K.V Ravi, 2nd International conference on the applications of diamond films and related materials. Editors: M. Yoshikawa, M. Murakawa, pp 13, 1993.
6. M. Sakamoto, J.G. Endriz and D.r. Scifrres: Electron. Lett., 28 (1992) 197.
7. R.F. Davis, Diamond films and coatings, (Noyce publications, Park Ridge, NJ),1993, pp 25-29.

8. K. Jagannadham, Journal of Vacuum Science and Technology, A 17 (2), Mar/Apr 1999.
9. V.P. Godbole, J. Narayan, Journal of Materials Research, Vol 11, N0.7, Jul 1996, pp 1810-1818.
10. K. Jagannadham, W.D. Fan, R.B. Dinwiddie, and J. Narayan, MRS symposium proceedings. Vol 445, pp51-55, 1997.
11. K.E. Goodson, O.W. Kading, M. Rosler, and R. Zachai, J. of Applied Physics, 77 (4), Feb 1995, p1385-1392.

Chapter 2

Literature Review.

In this section, a brief overview of the different forms of carbon, fundamentals of the growth techniques of diamond and aluminum nitride, and the characterization techniques performed in this research are given.

2.1 Forms of carbon

Carbon takes the following forms[1].

Diamond: Diamond usually occurs in the form of gemstones and has the face-centered diamond cubic structure as shown in fig.2.1.1[2]. Each carbon atom is tetrahedrally coordinated to four other carbon atoms as shown in fig.2.1.2[2] via sigma bonds emanating from sp^3 hybrid atomic orbitals. The four {111} directions in cubic diamond are in the bond directions. In any {111} direction the stacking sequence is ABC ABC ABC…The lattice constant is 3.56Å and the bond length is 1.54Å. The Raman spectrographic identifier signal for cubic diamond is at 1332cm^{-1} for carbon 12 and 1284cm^{-1} for carbon 13. Raman spectroscopy is based on the principle that the intensity of a beam of light decreases measurably when it passes through a non-absorbing medium. It is based on inelastic light-scattering arising from the interactions of photons with lattice vibrations or phonons. A laser tuned to a single light is used to excite the Raman scattering. The phonons are coupled to the photons through the polarization induced in the crystal by the electric field of the intense beam. A lattice vibration is Raman active when the vibration changes the polarizability. Some photons will be emitted from the induced oscillating dipoles that are either of the same frequency as the incident beam or have been shifted in frequency by an amount equal to the vibrational frequency of the lattice. The shifted frequency is the Raman scattering. The vibrational modes are dependent on the atomic

bonding in the solid. Therefore, Raman spectra can be used to interpret the structure of the solids.

Graphite: This is the most common form of carbon. The carbon atoms are trigonally bonded using sp^2 hybrid atomic orbitals. Each carbon atom exhibits three in-plane sigma bonds, and the remaining electron forms pi bonds using a p_z atomic orbital. Each plane is staggered from the planes above and below resulting in an AB AB AB ..sequence. In plane nearest spacing is 1.42Å while the lattice constant in the basal plane (between repeating layers) is 6.707Å. The Raman signal for graphite is $1580cm^{-1}$.

The other forms of carbon include lonsdaleite, microcrystalline carbon, amorphous carbon, carbon nanotubes, fullerene.

2.2 Growth of diamond

2.2.1 High pressure growth of diamond:

The drive for the high pressure growth of diamond was based on the fact that diamond is a high-density form of carbon (3.52gm/cc), and it seemed to be produced at high pressure because high pressure produces a smaller volume and hence a higher density, thus enhancing diamond growth[3]. However, there are three major problems in the high-pressure growth of diamond. First, extreme high pressures are required to achieve the compact, strongly bonded structure of diamond. Second, high temperatures are needed to make the conversion from other forms of carbon to diamond proceed at a useful rapid rate. Third, the diamond though obtained from above conditions is in the form of very small grains and another set of constraints are required to achieve the growth of large single crystals of diamond.

The carbon phase diagram[3,4]: From the phase diagram in Fig.2.2.1, it can be seen that graphite is the stable from of carbon all the way up to the melting curve near 4000^0C. If diamond is heated above 1500^oC at ambient pressure in the absence of air, it will convert to graphite and remain as graphite. The region of diamond stability can be noticed in the figure as opposed to graphite Fig. 2.2.1. Favorable conditions of diamond growth are shown identifying the choice of deposition at a particular temperature and pressure. The high-pressure synthesis of diamond identified as the Catalytic HPHT (High Pressure High Temperature) synthesis was initially performed by General Electric. Diamond growth can be achieved at pressures as low as one million psi and temperature below 2000^0C if a metallic solvent is used. Addition of some metals like Ni that act as a solvent by which graphite is dissolved is favorable at temperatures lower than 2000^0C. Diamond crystallizes out from the liquid metal due to its very low solubility. Diamond can be grown without using metallic solvents at high temperatures and pressures in the region identified as HPHT synthesis of the phase diagram. Thin film growth of diamond at low to ambient pressures as in chemical vapor deposition (CVD) takes place in the region showing meta stable CVD diamond. The major difficulty in diamond growth in the catalytic HPHT region is the achievement of both high pressures and temperatures simultaneously. After painstaking research by Bridgman, Hall, Bundy et al[3], in designing the appropriate equipment for producing both high pressures and temperatures simultaneously, growth of diamond became feasible. Large single crystal diamond could be grown using seed crystals but it usually takes a very long time to achieve a reasonable crystal size of 2-3mm.

2.2.2 Chemical Vapor Deposition (CVD) of diamond:

The CVD growth environment is described from Fig 2.2.2.1. The reactants, methane and hydrogen enter a high temperature or energetic region wherein the gas mixture is activated by a plasma triggered by a hot filament, by microwaves or a combustion flame front. A number of chemical reactions dissociating methane are initiated in this region and the resulting species are transported by forced flow, diffusion, and convection throughout the reactor, eventually reaching the substrate or being exhausted from the reactor. Near the substrate the species may diffuse through a stagnant flow region called the boundary layer. On the substrate surface, various processes may occur, such as adsorption, desorption, surface and bulk diffusion of species, as well as chemical reactions. Some are detrimental and other advantageous to diamond growth. Hence, diamond growth is a strong function of surface temperature, structure and composition of the substrate. The preferential formation and growth of the metastable diamond phase with sp^3 bonding of carbon atoms in preference to graphite with sp^2 bonding is the basic mechanism behind the CVD diamond growth.

Diamond nucleation during CVD process occurs as a result of suppression of graphite nucleus formation, stabilization of diamond nuclei and surfaces with respect to graphite nuclei and surfaces, and preferential etching of sp^2 carbon[5,6,7,8,9]. Molecular hydrogen reduces the partial pressure of gas phase species favorable to graphite nucleation[10]. The following are the general characteristics of CVD diamond growth[11]:

1. A gas phase must be activated either by high temperature or by plasma excitation or both.

2. The gas phase must contain a carbon-containing species such as hydrocarbon, an alcohol, carbon monoxide, or carbon dioxide.
3. There must be a sufficiently high concentration of species that etch graphite and/or suppress gaseous graphite precursors. Most commonly, this species is atomic hydrogen, H. Other graphite inhibitors include $(OH)^-$, O_2, atomic oxygen and F_2.
4. The substrate surface must be free from any catalysts that promote formation of graphite and be at or near the solubility limit for carbon at the deposition temperature. These conditions support the precipitation of diamond instead of the diffusion of carbon into the substrate. Initial carburizing of the surface such as the formation of a thin layer of SiC on Si will be helpful in achieving this objective[12].
5. A temperature gradient provides a driving force for the motion of diamond-producing species from gas phase to the substrate surface via diffusion because the activated gas phase is typically much hotter than the substrate surface.

2.2.2.1 Chemical vapor deposition methods[13]

Hydrocarbon pyrolysis:

This was the first method to demonstrate the chemical vapor deposition of diamond. This method is based on the theory that a diamond surface provides a crystal growth template for carbon descending from the vapor phase. The driving force for carbon to conform to the diamond template exceeds the driving force for carbon to revert to the thermodynamically stable graphite. The method consists of the pyrolysis of a pure hydrocarbon like methane, deposited diamond and non-diamond carbons onto a diamond substrate. This deposition step is followed by selective etching of non-diamond carbon

from the deposit by molecular hydrogen, and the reaction cycle repeats. Rate of deposition is slow in this method.

Fluorocarbon pyrolysis:

This method is based on the fact that graphite etching is enhanced by presence of OH radicals, O_2, O^0, F_2, and F^0. The pyrolysis of fluorocarbons such as CF_4 leads to the deposition of diamond. A mixture of CF_4 and F_2 diluted in He is blown onto a diamond substrate surface. The substrate is heated to 875^0C by a resistance heater. No plasma activation, hot filament activation, or electric field activation of the gas phase is required for this growth. This is a very efficient method of diamond growth with a deposition rate of 0.6μm/hr. But the corrosive nature of CF_4 and F_2 limit the use of this method in diamond deposition.

Heated filament method: The basic mechanism behind this technique is the formation of atomic hydrogen by passage of H_2 over a refractory metal filament, such as tungsten, heated to temperatures between 2000 to 2300^0C. Atomic hydrogen helps to etch away graphite while enhancing the formation of diamond. At high temperatures like 2000^0C, methane decomposes into acetylene species, methyl radicals and other hydrocarbons stable at high temperatures, and H_2 decomposes into H^0.

$$2CH_4 = C_2H_2 + 3H_2.$$

After acetylene diffuses to the substrate, solid carbon precipitates on the substrate surface in order to reduce the super-equilibrium concentration of the species such as acetylene in the gas phase. The diamond allotrope of carbon is stabilized by a concurrent super-equilibrium concentration of H^0. However, the exact nature of the reaction kinetics that occur in the diamond deposition are not yet definitive and still being debated. It has also

been found that the addition of trace amounts of oxygen or oxygen bearing species tends to expand the temperature range over which the diamond deposition occurs and increase the deposition rate. The advantages of this method include high deposition rates up to 1μm/hr, low cost, and its ability to accommodate the use of a wide variety of carbon-bearing source gases.

Plasma enhanced chemical vapor deposition:

The mechanism behind plasma enhanced chemical vapor deposition is based on the fact that the concentration of atomic hydrogen and subsequent graphite etching can be increased by the use of an electrical discharge or plasma. Different plasma frequencies are obtained; microwave plasma CVD uses excitation frequencies of 2.45GHz, and radio frequency (RF) plasma excitation employs frequencies of 13.56 MHz.

Microwave plasma enhanced CVD: Microwave plasmas are different from other plasmas in that the microwave frequency can oscillate electrons. Collision of electrons with gas atoms and molecules generates high ionization fractions. This method to grow diamond films was first demonstrated by a research group in Japan's National Institute for Research in Inorganic Materials, NIRIM. Microwaves can be generated either by a proprietary antenna, or by a magnetron, go through a circulator, a stub tuner, pass through a quartz microwave window before entering the PECVD process chamber. The substrate is placed on a platen that is usually electrically conducting and will couple to the microwaves, stabilize the plasma and become heated. The platen is also heated by an external DC source up to around 350^0C. Sometimes the platen is a small graphite block. The typical deposition parameters for microwave plasma enhanced CVD are as follows: gas composition between 0.1 to 5% CH_4 diluted in H_2; total flow rate between 50 and

500sccm; substrate temperature between 400 and 1000^0C; total pressure, between 1 and 400 torr.

RF Plasma enhanced CVD: Radio frequency power can be applied to create a plasma by a capacitively coupled parallel plate or by induction. The frequencies usually employed in RF plasma enhanced CVD are 13.56MHz. The advantage with RF plasma is that it can be produced over a large area when compared to microwave plasma and hence larger substrates can be used. Ion bombardment from the plasma can create diamond-like hydrocarbon films. Capacitively coupled RF plasmas are used for the synthesis of diamond films.

DC plasma enhanced CVD: In DC plasma enhanced CVD, a negative or positive DC voltage is applied to the substrate platen or to an auxiliary electrode respectively. Intermediate electrodes may be used to guide the plasma and alter the plasma position and properties. This method has the advantage of growing diamond over large areas but the plasma gets self-extinguished if a very thick film of the dielectric diamond is deposited on the platen because it changes the bias. The advantage with DC plasma enhanced CVD is that very high growth rates up to 80μm/hr can be achieved. Growth rates of up to 200-250μm/hr were also reported. The mechanism of this method is that an arc of the reactant gases is sustained above the substrate by a certain amount of power. The input gas composition is usually CH_4+H_2 with a carrier gas of Ar or He.

Other methods of diamond deposition include the physical vapor deposition techniques by arc evaporation, electron beam evaporation or sputtering of solid carbon sources like graphite, soot and amorphous carbon. Diamond also could be synthesized by combustion wherein diamond particles deposited beneath the center of an oxy-acetylene

torch placed onto a substrate. Diamond crystallites are observed to nucleate and grow where the luminous cone of the flame intersects a surface cooled to about 800-1050^{0}C.

2.3 Growth of aluminum nitride

Aluminum nitride is considered useful in integrated electronic circuits because of its good dielectric properties coupled with fairly good thermal conductivity. Apart form this, AlN being a wide bandgap semiconductor is also used in the fabrication of blue light emitting diodes. The other important properties of AlN include high surface acoustic velocity, high dielectric constant, high temperature stability and hardness[14]. The properties of AlN are listed in Table 2.3.1[15]. The structure of AlN is shown in figure 2.3.1[16]. AlN has a hexagonal close packed (HCP) structure. The AlN HCP lattice is visualized as a top and bottom plane of 7 atoms of aluminum forming a regular hexagon around a central atom. In between these planes is a half-hexagon of 3 atoms of nitrogen. The Al, and N atoms are stacked in the ABABAB…sequence. The fairly good thermal conductivity of AlN enables its use as a heat sink in electronic packaging. However, diamond scores over AlN as a heat sink material due to its very high thermal conductivity which is almost ten times that of AlN and its thermal expansion is about 2-3 times lower than that of AlN. The maximum temperature rise above heat sink for CVD diamond is 12 times lower than that for AlN, for the same thickness of the films. However, the use of diamond as a substrate in electronic circuits needs moderate thickness, homogenity, and large size that is difficult to grow at a low cost[17]. The low pressure synthesis of diamond, although helping to cut down on the costs involving the growth of diamond, is by itself not sufficient to dissipate the heat as the heat capacity of diamond is low, 6.19 Joules/moles-^{o}C [18]. The use of aluminum nitride counters the disadvantage of the loss of

thermal conductivity of diamond because of the presence of voids and discontinuities. In addition, it also improves the adhesion of the first layer of discontinuous diamond to the subsequent deposited layers[19]. Aluminum nitride can also be used as a buffer layer for diamond growth on Si and steel and prevents diffusion of carbon in to Si and steel from the gaseous atmosphere during the growth of diamond. The presence of aluminum nitride enhances the nucleation of diamond in HFCVD[20]. This is based on the conclusion that the AlN surface had undergone some kind of chemical reaction with the CVD gas environment to provide sites for heterogenous diamond nucleation.

Epitaxial aluminum nitride was grown on Si (111) substrates by RF magnetron sputtering at high temperatures ranging from 700^{o}C to 1000^{o}C. The films grown are highly oriented or of basal plane (002) orientation. High quality crystalline aluminum nitride cannot be grown very easily because of the residual oxygen contamination that is very difficult to avoid. However, good quality AlN growth can be achieved in ultra-high vacuum conditions with very little contamination from oxygen[21]. The effect of temperature, sputtering power, pressure and the percentage of N_2 on the growth of AlN was studied in detail by Chein-chuan et al[22]. The best conditions for the growth of highly c-axis oriented AlN thin films on Si (100) substrates by rf magnetron sputtering were a sputtering pressure of 7.5 mtorr, N_2 concentration of 75%, rf power of 300W, and substrate temperature of 350^{o}C. The films are reported to have an average grain size of 100nm. The percentage of nitrogen in the sputtering gas plays an important role in the growth orientation of the films and higher nitrogen enhances the (002) orientation. Less N_2 decreased the crystalline quality of the films, and resulted in different growth orientations like (100) and (101). However, at a constant percentage of N_2 at 25% of the

gas mixture, the preferred orientation of AlN films grown by RF sputtering can be altered by the presence of hydrogen[23]. A strong (002) orientation was observed with the increase in hydrogen percent from 0-20% when the nitrogen concentration was kept constant at 25%. The orientation of the films changed from (100) at very low percentage of H_2, to (002) at about 20%. Epitaxial growth of aluminum nitride on Si(111) by dc reactive magnetron sputtering at 500-800^{o}C has been reported[24]. The results indicate that temperature plays a very important role in epitaxial growth of AlN. The orientation changed from highly textured at 500^{o}C to a single crystal, at and above 600^{o}C as observed by transmission electron microscopy. The films follow the epitaxial relationship AlN [0001]//Si[111]. Aluminum nitride can also be deposited by reactive partially ionized beam deposition (PIB) using Al as evaporation material and N_2 as reactive gas at a temperature as high as 500-600^{o}C similar to reactive magnetron sputtering[25]. However, unlike sputtering which uses Ar^{+} ions to bombard the surface during growth, the PIB technique utilizes self-ions, i.e, the ions of the deposited material, to assist film growth. In this method the high purity metal is evaporated, and the evaporated species and the reactive gas are partially ionized by electron bombardment of the ionization zone. The dissociated and activated aluminum and nitrogen containing species are accelerated to the substrate in the acceleration field.

Chemical vapor deposition of AlN is usually carried out at higher temperatures around 800 to 1100^{o}C[26,27]. This method gives high purity AlN films with low or practically zero amounts of oxygen. The smoothness of the films is also increased in the case of MOCVD because of insitu etching of the substrate by the precursors. The precursors used are $AlCl_3$ or $Al(CH)_3$, N_2, and NH_3. Layer by layer growth of AlN was

performed by molecular beam epitaxy[28], and by plasma assisted gas source epitaxy[29]. Pulsed laser deposition is used to deposit aluminum nitride[14,30]. A compound AlN target is ablated using a KrF laser source (λ = 248nm) in an ultra-high vacuum environment with a substrate temperature maintained at 600^{o}C. The basal plane (002) growth orientation of AlN was observed in all these cases.

In implementing the idea of composite heat spreader coatings, the method we chose for the deposition of diamond was microwave plasma enhanced chemical vapor deposition (MPECVD), and dc reactive magnetron sputtering for aluminum nitride. The depositions were followed by characterization of the films. All the techniques used for deposition and characterization are discussed briefly in the following sections.

2.4 Deposition techniques:

Deposition of aluminum nitride by DC reactive magnetron sputtering[31]:

AlN was deposited onto the samples by pulsed DC reactive magnetron sputtering (RMS). In the sputter system an inert gas is fed into the deposition chamber at low pressure. A DC voltage is applied across two electrodes using a pulsed DC power source and a plasma is created. The plasma contains neutral argon atoms, positive ions, free electrons and it is a conducting medium. The target material to be deposited is negatively biased by applying a negative DC voltage. The substrate and the chamber walls act as the anode. Once the plasma is created, the positive ions in the plasma are accelerated to the negatively biased target. These energetic ions strike the target and sputter away the target atoms. The sputtered atoms ionize, travel through the plasma and strike the surface of the substrate and the chamber walls where they condense and form the deposited film. To increase the efficiency of the ionization from the collisions between the electrons and gas

atoms, magnets are used behind the target in magnetron sputtering. The magnetic field perpendicular to the electric field traps electrons near the target surface, and causes them to move in a spiral motion until they collide with an argon atom. The ionization and sputtering efficiencies are increased and great deposition efficiencies are achieved in reactive magnetron sputtering (RMS). In pulsed DC magnetron sputtering, an electron trap is formed over the surface and intense plasma is generated[14]. This results in increased deposition rates, a very good advantage of using pulsed DC RMS. However, the surface of the chamber will also get deposited with the insulating AlN film calling for cleaning the chamber after every deposition. In RMS, the recorded effective and collected powers are an indication of the metallic nature of the films. The effective power accounts for the ions in the plasma whereas the circulating power is that applied to generate the plasma. A higher effective power than the circulating power implies metallic nature of the film while a higher circulating power than the effective power implies insulating nature of the films[14].

Deposition of diamond:

Diamond was deposited by the microwave plasma enhanced CVD technique (MPCVD), the details of which have been described in section 2.2. However, prior to diamond deposition, the surface of the substrate should be conducive for better diamond nucleation and growth. For better nucleation of diamond, the surface of the substrate should be clean with the primary requirement of the absence of any graphitizer or graphite nucleants. Scratching the substrate, applying diamond powder crystallites on the surface of the substrate prior to the deposition enhances diamond growth. Nucleation also occurs at

steps, ledges, screw dislocations[32], grain boundaries[20]. The surface preparation details employed are discussed in the following chapter.

Silicon nitride deposition:

Diamond oxidizes in the presence of O_2 above 600^{o}C. Hence, it is imperative that the diamond is protected during device processing. Silicon nitride is a good diffusion barrier for oxygen and can be deposited on the diamond side to achieve this purpose.

The deposition of silicon nitride was carried out by low pressure chemical vapor deposition (LPCVD)[33]. LPCVD is based on the principle that lowering the total pressure of the gas stream increases the diffusion of gases through the boundary layer and equal fluxes of reactant gases reach the surface of the substrate in order to achieve a uniform deposition. The CVD film deposition rate is given by

$$\nu = (k_s h_g C_t Y)/(k_s + h_g)N$$

where k_s is the surface reaction coefficient, h_g is the mass transfer coefficient, N is the number of atoms incorporated per unit volume in the film, C_t is the concentration of all the gases in the gas phase, and Y is equal to the partial pressure of the incorporating species divided by the total pressure in the system. The mass transfer coefficient is given by

$$h_g = D_g/\delta_s$$

where, D_g is the diffusivity of the reacting species through the boundary layer and δ_s, the boundary layer thickness. The diffusivity is inversely proportional to the total pressure or the number of collisions that the gas species experience. Therefore, decreasing the total pressure increases D_g and h_g. The deposition is dominated by the surface reaction, and generally limited by the temperature across the substrate. The chamber ambient is

maintained at 0.25-2 Torr range, and the deposition temperature range from 300-900^{o}C. Diamond oxidizes to form carbon dioxide in the presence of oxygen above 600^{o}C. The two most important high temperature steps in electronic device processing are the growth of field and gate oxides. Hence, it is important to protect the backside diamond during device integration. A thin diffusion barrier coating on diamond protects it from oxidation. Silicon nitride is an excellent diffusion barrier for oxygen and therefore a film of thickness 1600Å was deposited on the diamond. The experimental details of the deposition are discussed in the next chapter.

Etching of silicon nitride[34]:

To ensure that the device side is free of any films, silicon nitride needs to be etched. There are two methods for etching silicon nitride, chemical and dry etching. Chemical etching, uses a boiling solution of phosphoric acid and water at a temperature of 130-150^{o}C. This method is not suitable with a mask because photoresist decomposes above 100^{o}C. The second method is dry or plasma etching. In this method, a low pressure gas (1 mtorr to1 torr) is used in the chamber. By applying a high electric field across two electrodes, some of the gas atoms are ionized, producing positive ions and free electrons and creating a plasma. The choice of the gas composition is based on the film to be etched, the etch rate and the selectivity of the gas composition. When the wafers are placed on a smaller electrode, the etching is said to be operating in the Reactive Ion Etching or RIE mode. RIE systems operate usually in the 10 to100 mTorr range. RIE mode of operation results in stronger ion-bombardment and higher etch rates.

Field oxide growth:

The two common oxidation steps in the silicon device technology are the growth of field oxide and the gate oxide. In order to integrate the diamond heat spreaders with device wafers, it is necessary to examine the stability of diamond after oxidation and also if this high temperature step will cause any diffusion of carbon and other species from the diamond film into the wafer. The stability of diamond in the composite heat spreader was observed by scanning electron microscopy, the details and the results of which are described in the following chapters.

2.5 Characterization techniques

2.5.1 I-V characteristics of a Schottky diode[35,36]:

The I-V characteristics of a Schottky diode show a high current in the forward bias and very low or practically no current in the reverse bias. The forward current is due to the injection of majority carriers from the semiconductor into the metal. In the case of a Schottky contact between an n-type semiconductor and a metal with higher work function when a forward bias is applied, electrons in the semiconductor conduction band can diffuse across the depletion region into the metal. This gives rise to a forward current (metal to semiconductor) through the junction. A reverse bias increases the barrier and electron flow becomes negligible. The analogy can be extended to a Schottky contact between a p-type semiconductor and a metal with a lower work function than the semiconductor in which case the majority carriers are holes. In case of an ideal Schottky diode, the Schottky barrier height is given by the equation

$$\phi_b = \phi_m - \chi$$

where ϕ_b is the Schottky barrier height and $q\chi$ is the electron affinity of the semiconductor measured from the top of the conduction band to the vacuum level. From the I-V characteristics of a Schottky diode, ϕ_b is determined by measuring the current density, J, in terms of the applied voltage, V, across a Schottky barrier. J is related to V by the equation

$$J = AT^2[\exp(-q\phi_b/kT)][\exp(qV/nkT)-1]$$

In this equation, n is the diode ideality factor, which is unity for the ideal Schottky barrier diode. The plots of J versus V (in the forward bias condition allow the determination of both ϕ_b and n. The intercept at V = 0 yields the saturation current that gives ϕ_b. The slope of the linear region when I-V characteristics are plotted on a logarithmic scale gives the value of n. The current-voltage characteristics of a Schottky diode are very sensitive to surface preparations and subsequent changes induced at the interface by a processing treatment such as annealing at high temperature. This is because the presence of surface states at the free surface of the semiconductor could behave like a metal on the surface. These states may trap an electron from the bulk of the semiconductor. The presence of these states causes the image force lowering of the barrier and this leads to a lower barrier height. Thus, the surface states reduce the barrier height.

2.5.2 Deep Level Transient Spectroscopy (DLTS)[37]:

DLTS is a capacitance measurement technique used to detect the electrically active impurities, complexes, defect energy levels, and traps in the substrate. The method uses the capacitance of a p-n junction or Schottky barrier diode as a probe to monitor the changes in the charge state of the centers. The DLTS measurement consists of a sensitive capacitance measurement apparatus with good transient response, one or two pulse

generators to make rapid changes in the diode bias, a dual gate signal integrator, and an X-Y recorder, and a variable temperature cryostat. The presence of each trap is indicated by a positive or negative peak of the capacitance gradient on a flat baseline plotted as a function of temperature. The heights of these peaks are proportional to their respective trap concentrations, the sign of each peak indicates whether it is due to a majority or minority carrier trap, and the positions of the peak are determined by the integrator gate settings and the thermal emission properties of the respective traps. By the proper choice of experimental parameters, it is possible to measure the thermal emission rate, activation energy, concentration profiles, and capture rate of each trap.

2.5.3 Secondary ion mass spectroscopy[38]:

Secondary ion mass spectroscopy is an analytical spectroscopy technique used to detect and quantify low-level impurities in the substrate. It is felt essential to detect the concentration of oxygen and carbon in the substrate after diamond deposition. Diamond deposition was performed in microwave PECVD is initiated in low vacuum conditions of $5.5X10^{-3}$ Torr for long periods of time (25-30 hrs) at 900-950^{o}C. Diffusion of impurities along with the gaseous species, especially oxygen, and carbon coming from the gaseous environment is possible. Also, it is felt necessary to determine the carbon concentration on the device side of the substrate. Carbon may have diffused from the source methane gas, or from the graphite block below. Hence SIMS analysis has been performed on the device side of the samples to check for the concentration of carbon, oxygen, nitrogen, and hydrogen by depth profiling to 3-5μm. Sputtering of the sample surface with a primary ion beam followed by mass spectrometry of the emitted secondary ions constitutes secondary ion mass spectrometry (SIMS). As a result of ion impact, atomic and

molecular species, electrons, and photons are emitted from the surface. In SIMS, only the secondary ion emission is studied for surface analysis. The secondary atomic and molecular particles originate from an emission zone. The atomic and molecular ions may also come from deeper layers if they have sufficient kinetic energy. The secondary electrons and photons can also be used for surface characterization in other methods like AES, XPS, etc to determine the chemical composition of a surface. Secondary ions produced by sputtering are extracted from the sample. If large mass spectrometer components are held at ground potential, the sample must be held at high voltage, or the accelerating potential. The secondary ions accelerate toward the ground plate of an electrostatic lens. This first lens is called the immersion or ion extraction lens. The second (transfer lens) focuses the ion beam onto the mass spectrometer entrance slits or aperture. This two-lens system constitutes an ion microscope. The secondary ions could be projected onto an image detector for viewing the sample surface. Different transfer lenses produce different magnifications. The secondary ions are mass analyzed using quadrupole mass analyzers and detected using single ion counters or faraday cup. Thus, the specific ions corresponding to the specific elements can be detected efficiently with this method giving a quantitative analysis of the impurities present on the surface of the sample.

2.5.4 Electron microscopy:

The principle of electron microscopy is based on the fact that electron wavelengths in the order of atomic dimensions, can be used to observe the microscopic features with a very high resolution. The image resolution of TEM can be related to the Rayleigh criterion for light microscopy, which states that the smallest distance that can be resolved, δ, is given

approximately by the equation $\delta = 0.61\lambda/\mu \sin\beta$, where λ is the wavelength of the radiation, μ the refractive index of the medium, and β is the semi-angle of collection of the magnifying lens. From DeBroglie's equation, $\lambda \sim 1.22/E^{1/2}$, where E is the energy of the electrons in electron volts, and λ the wavelength in nm, we can go to very small wavelengths by increasing the energy. Electrons are one type of ionizing radiation with the advantage that it produces a wide range of secondary signals from the specimen. From these signals, the method of the electron microscopy is applied. The secondary electrons and the backscattered electrons generated from the surface are used in scanning electron microscopy to observe the surface features and morphology. The transmitted electrons that are the elastically and inelastically scattered are used in transmission electron microscopy to extract information about the atomic arrangement and composition. Momentum to the electrons is imparted by accelerating it through a potential drop, V. The electron source can be either the field emission source or the thermal emission source. The accelerated electrons are used with electron-optics consisting of electromagnetic lens; condenser, objective, and intermediate lenses. Imaging using diffraction or strain contrast and phase contrast is performed onto a fluoroscent screen. Electron diffraction is also carried out using the small electron wavelengths and flat Ewald sphere construction in the reciprocal lattice.

2.5.5 Heat spreading characteristics:

The heat spreading characteristics were determined by infrared thermography using the facilities at the high temperature materials laboratory in Oak Ridge National Laboratory. The technique consists of localized heating of the sample in a small region (spot) and imaging the temperature variation of a point separated from the heated spot. Thus, the

heat spreading capability of the substrate can be studied. This can correspond to the real-time scenario of spreading the heat produced during the operation of a high power device. The variation in temperature of a chosen point separated from the heated spot is measured by the variation in the colors seen on the pixels of the images captured by an infrared camera. The images can be calibrated with respect to intensity that is directly proportional to the temperature at any point. The temperature variation is plotted as a function of time. The raise in temperature of a particular point away from the heater indicates the amount of heat that is spreading from the resistor laterally into the sample. Thus, the higher the increase in observed temperature, the better are the heat spreader characteristics.

The following chapter gives the experimental details of all steps in deposition, device integration and characterization. This is followed by the analysis of all the results obtained and the conclusions derived from these results is discussed in the final chapter.

References

1. R.F. Davis, Diamond films and coatings, development, properties and applications (Noyce publications, Park Ridge, 1993) pp 2-3.
2. Website: **www.uwgb.edu/dutchs/PETROLGY/ Diamond%20Structure.HTM**
3. R.F. Davis, Diamond films and coatings, development, properties and applications (Noyce publications, Park Ridge, 1993) pp 34-35.
4. Website: http://www.me.berkeley.edu/diamond/submissions/diam_intro/cphased.htm
5. D.V, Fedosayev, B.V. Deryagin, and I.G. Varasavskaja, Surface and coatings technology 38(1-2): 1-130 (1989).
6. B.V. Deryagin and D.V, Fedosayev., Surface and coatings technology 38(1-2): 132-248 (1989).
7. W.A. Yardborough and R. Messier, Science (247): 688-696 (1990).
8. E.S. Machlin, Journal of Material research 3 (5): 958-968 (1988).
9. T.R. Anthony, Vacuum 41(4-6): 1356-1359 (1990).
10. W. Piekarczyk, R. Roy, and R. Messier, Journal of crystal growth 98: 765-776 (1989).
11. R.F. Davis, Diamond films and coatings, development, properties and applications (Noyce publications, Park Ridge, 1993) pp 148-149.
12. P.O. Joffreau, R. Haubner, and B. Lux, MRS symposium proceedings, Vol. EA-15, p.15, Pittsburgh, PA (1988).
13. R.F. Davis, Diamond films and coatings, development, properties and applications (Noyce publications, Park Ridge, 1993) pp 150-177.

14. K. Jagannadham, A.K. Sharma, Q. Wei, R. Kalyanaraman, and J. Narayan, Journal of vacuum science and technology, A 16 (5), Sep/Oct 1998.
15. Website: http://www.accuratus.com/Aluminum_Nitride.htm
16. Website: www.jwave.vt.edu/crcd/farkas/ lectures/structure/fig3.gif
17. J.B. cui, Y.R. Ma, J.F. Zhang, H. Chen, R.C. Fang, (submitted paper).
18. K. Jagannadham, solid state electronics,Vol. 00, No. 0, pp 1-10, 1998.
19. K. Jagannadham, Journal of vacuum science and technology A, 17(2), Mar/Apr 1999.
20. V.P. Godbole, J. Narayan, Journal of Materials Research, Vol 11, N0.7, Jul 1996, pp 1810-1818.
21. F. Malengru and M. Veremeersch, Journal of material research, vol 12 No.1, Jan 1997, pp 175-188.
22. C. Chuan, Y.C. Chen, H.J. Wang, W.R. Chen, Journal of vacuum science and technology A, 14 (4), Jul/Aug(1996), pp 2238-2243.
23. H.C. Lee, K.Y. Lee, Y.J. Yong, J.Y. Lee, G.H. Kim, Thin solid films 271, pp 50-55, 1998.
24. W.J. Meng, J. Heremans, and Y.T . Cheng, Applied physics letters. Vol 59(17), October 1991, pp 2097-2099.
25. J. Xie, Q. Mo, and J. Feng, Nuclear instruments and methods in Physics Research B, vol 124, pp519-522, 1997.
26. C. Li, L. Hu, W. Yuan, and M. Chen, Materials chemistry and physics 47, pp273-278, (1997).
27. R.C. Buggeln, M. Meyyappan, and S.J, Shamroth, Journal of vacuum science and technology A, 14(4), Jul/Aug 1996.

28. B. Daundin and F. Widmann, Journal of crystal growth 182, pp1-5, 1997.
29. A, Bourret, A. Barski, J.L. Rouviere, G. Renaud, and A. Barbier, Journal of applied physics, vol 83, No. 4.
30. T. Ogawa.M. Okamoto, H. Yagi, Y. Mori, A. Hatta, T. Ito, T. Sasaki, A Hiraki, Diamond films and technology, Vol 6, No.2, pp 87-94 .
31. J.D. Plummer, M.D. Deal, and P.B. Griffin, Silicon VLSI Technology (Prentice Hall, New Jersey)pp539-551.
32. R.F. Davis, Diamond films and coatings, development, properties and applications (Noyce publications, Park Ridge, 1993) pp 90-93.
33. Plummer, Deal, and Griffin, J.D. Plummer, M.D. Deal, and P.B. Griffin, Silicon VLSI Technology (Prentice Hall, New Jersey)pp512-521.
34. J.D. Plummer, M.D. Deal, and P.B. Griffin, Silicon VLSI Technology (Prentice Hall, New Jersey)pp631-633.
35. B.G. Streetman, Solid State Electronic Devices, (Prentice Hall, India, 1997), p184.
36. S.P. Murarka, Metallization, theory and practice for VLSI and ULSI. (Butterworth-Hienemann, Boston) 1993, pp 54-55.
37. D.V. Lang, Journal of applied physics, Vol.45, No.7, July 1974.
38. A Benninghoven, Surface Science, 53 (1975) 596-625.

Chapter 3

Experimental details

3.1 Growth

This chapter gives the experimental details of the preparation of the substrates, deposition, and characterization of the heat spreader. The process flow of all the steps in proving the device integration is shown in appendix 1.

3.1 Substrate surface preparation:

The substrate should be atomically clean because the contaminant films and impurities can get into the thin films or into the silicon itself. The surface contaminants also affect the growth and orientation of the films. The presence of an amorphous oxide on the surface of the substrate makes the film grow polycrystalline during deposition that is not desirable. A p-type silicon (100) wafer coated with silicon nitride with an average thickness of 1600Å was chosen as the substrate. The substrate preparation included several steps. First, the substrates were cleaned with acetone to dissolve any surface contaminants like grease, oils, etc. The substrates were cleaned with methanol to remove any residue after cleaning with acetone. Further, the wafer samples were rinsed in distilled water. As a next step, the silicon nitride on the backside (unpolished side) of the wafer was etched in 49% hydrofluoric acid for about 25 minutes, followed by rinsing in distilled water and drying. This procedure is also designed to etch away the underlying oxide as well. The substrate is ready for deposition of AlN.

3.2 Deposition of aluminum nitride:

AlN was deposited on the backside (Si_3N_4 etched) by dc reactive magnetron sputtering method using ultrahigh purity argon at partial pressure of 0-1mtorr and nitrogen gas mixture, with the total pressure of 1-2mtorr in the chamber. A 4inch aluminum target of 99.999% powered by a pulsed DC source was used. The stainless steel chamber was

evacuated to a predeposition vacuum of $5X10^{-6}$ torr. The substrate was heated to 600^{o}C using a pulsed DC power source, and the temperature measured by a thermocouple placed on the ceramic substrate holder. The shutter was closed for the initial two minutes of cleaning the target. Cleaning was done in an argon plasma with Ar pressure of 0-1 mtorr. The target current applied was 0.5A in the cleaning stage. A target current of 2A was applied, and the ratio of circulating to effective power was 1.05kW to 0.62kW. The significance of effective and collective powers has been described earlier in section 2.4. These ratios indicate the insulating nature of the film being deposited that is as expected because aluminum nitride is an insulating film. The deposition time was varied between 30-90 minutes.

3.3 Diamond deposition:

The Si substrates with aluminum nitride film were first cleaned using acetone and methanol. Further, the substrates were given an ultrasonic suspension of 1μm industrial diamond powder in an acetone bath. After loading the sample, the microwave plasma deposition chamber was evacuated to a pressure of $5.5x10^{-3}$ torr. The chamber is equipped with a 1.5 kW Astex scientific microwave source operating at 2.45Ghz. The substrate was placed on graphite block placed on the platen. The graphite block absorbs the microwave power and stabilizes the microwave plasma. The graphite/substrate was heated up to a temperature of 300-350^{o}C by a dc heater. The temperature of the graphite block was measured by placing a thermocouple just below the platen. After the temperature reached around 300^{o}C, hydrogen was introduced into the chamber through a mass flow meter at 160 sccm. The microwave plasma was turned on at 900W when the partial pressure reached 12-13 torr. The pressure is slowly increased up to 35 torr. The

temperature increases and stabilizes around 900^{o}C. Methane was released into the chamber at 0.8sccm through a mass flow meter controlled by a mass flow controller. The pressure in the chamber was regulated at a constant value of 35 Torr. The CH_4/H_2 ratio was 0.5% with the hydrogen flow at 160sccm and methane flow maintained at 0.8sccm. Deposition of diamond continued in steps of 12 hours for 25 hours for each sample. The applied forward power was 900W and the reflective power was regulated to remain between 0-3W by tuning the source. The thickness of the deposited diamond layer was about 25μm.

3.4 Silicon nitride deposition on the backside:

Silicon nitride is an excellent diffusion barrier for oxygen and therefore a film of thickness 1600Å was deposited on the diamond. This thickness was chosen because the etching steps after each device processing step also etch some amount of silicon nitride as well. The deposition was performed at a pressure of 300 mtorr in the class 100 clean room facility of AEMP center in NCSU. The samples were placed horizontally on a 4 inch silicon wafer on a quartz boat. The temperature was maintained at 775^{o}C, and the gas mixture consisted of NH_3, and SiH_2Cl_2. The total deposition time was 40 minutes. The gas flow rates were 120sccm for NH_3 and 40sccm for SiH_2Cl_2. The thickness measured by nanometrics on a monitor sample placed beside the substrates showed an average value of 1586Å. The device side also got deposited with the silicon nitride film although the samples were placed horizontally. The thickness of the film varied from a high value at the edges to a low value at the center of the sample on the device side.

3.5 Etching of silicon nitride on the device side:

The gas composition used for the reactive ion etching of the silicon nitride on the device side was the SF_6/O_2, each having a flow rate of 15 sccm. The total etching time and pressure were 10 minutes and 30 mTorr respectively.

3.6 Field oxide growth:

The AlN/diamond composite coated silicon, and the monitor or reference silicon that did not have any coating on it were oxidized to grow the field oxide. The oxide film was grown in a quartz furnace in the class 100 clean room facility of AEMP, NCSU. The samples were placed horizontally on a dummy silicon wafer and loaded into the furnace. The oxide growth cycle started with a temperature ramp up from 600-1000^oC for 35 minutes in N_2 flow of 7200 sccm, and O_2 flow of 200 sccm. The pre-oxidation consisted of O_2 flow for 10 minutes and 2% HCl flow at 61 sccm at 1000^oC. Then the wet oxidation was done in an O_2 flow of 1000 sccm, and H_2 flow of 2000 sccm for 14 minutes at 1000^oC. Post oxidation was for 10minutes with O_2 flow of 1000 sccm and HCl at 61 sccm at 1000^oC. Further, the samples were annealed at 1000^oC for 10 minutes followed by cooling in the presence of N_2 for 45 minutes. The thickness was measured by nanometrics and the average thickness of oxide on the monitor sample was 1596.33Å, and the average thickness on the composite coated sample was 1585.7Å. To facilitate the Schottky deposition, the samples were buffered oxide etched (BOE) again for 3minutes and 10 seconds.

3.7 Schottky diode fabrication:

To facilitate the DLTS measurements and to test for the device integration, fabrication of a Schottky diode on the device side was performed. The following steps were used in the Schottky device fabrication.

3.7.1 Polishing:

To obtain good quality Schottky diodes, the surface needs to perfectly clean, and smooth so that leakage currents in the reverse bias mode can be reduced. The surface of the sample after reactive ion etching was uneven because of the ion bombardment at the surface. This was corroborated by the inconsistent and erroneous thickness values measured by nanometrics. The nanometrics measurements use reflected and refracted light to determine the thickness of the sample and hence a very smooth surface is needed. The samples were polished before any further process steps. The polishing of the samples was carried out on disc polishers starting with 600 grit silicon carbide polishing paper, followed by 6μm, 3μm, 1μm diamond powder, and ending with a final polish using colloidal silica suspension. The time for each cycle was 20 minutes and the sample finally had a very shiny, smooth surface.

3.7.2 Piranha cleaning and etching of silicon dioxide:

In order to facilitate deposition of the Schottky contacts and DLTS measurements, the samples were subjected to a Piranha etch that included cleaning in a 1:1 solution of H_2SO_4 and H_2O_2 for about 10 minutes. The subsequently formed oxide layers were etched using a buffered oxide etch (BOE) solution for 3 minutes just before deposition.

3.7.3 Schottky deposition:

The metals chosen for Schottky deposition were Ti-Al. Using only aluminum caused diffusion problems and the contact exhibiting ohmic rather than Schottky character during earlier work. Therefore, Ti was used as the contact for the Schottky barrier. Using a resistance heating furnace, Ti (20nm) first and Al (~120nm) second were successively evaporated onto the samples using a shadow mask to form 1mm-diameter Schottky barrier diodes.

3.8 Characterization

3.8.1 Deep Level Transient Spectroscopy (DLTS):

A BioRad DL 8000 system was used to measure the DLTS signal in the temperature range from 30K to 300K. The samples were placed under a reverse bias of 3Vand a superimposed filling pulse of 3.5 V above the bias (pulse width was 1ms).

3.8.2 Secondary ion mass spectroscopy (SIMS):

SIMS analysis was performed on a CAMECA IMS-6f using a Cs^+ primary ion source and detection of negative secondary ions. The primary current was 212 nm, raster size 200 μm, and the voltage was 982 V. Three samples were loaded along with the standard sample used to determine the concentration. The samples loaded for examination were a) the monitor sample or the reference silicon that did not undergo any deposition, b) the composite coated sample, and c) the composite coated sample that underwent the oxidation step. All the samples were analyzed from the device side, and the impurity concentrations were compared with the monitor sample. Standard samples implanted with hydrogen, oxygen, carbon, and nitrogen were used for determining the concentrations of the respective elements in the samples.

3.8.3.1 Scanning electron microscopy :

Planar samples were used and there was no specific sample preparation necessary apart from the cleaning of the surface with acetone and methanol prior to the observation. Scanning electron microscopy was performed using the Hitachi environmental scanning electron microscope, Hitachi-ESEM. The samples were examined in the secondary electron mode. Two samples were examined: (a) Composite coated Si just after the growth of diamond (b) Composite coated Si after oxidation treatment to check for the stability of diamond. The applied voltage was 17kV for examining the morphology after diamond growth. The samples that were oxidized contained a silicon nitride coating on the diamond side so that a lower voltage of 12kV was used to avoid charging of surfaces.

3.8.3.2 Transmission electron microscopy:

Transmission electron microscopy calls for a very thin electron transparent sample. In order to visualize the growth characteristics of AlN and diamond, cross-section specimens were prepared. The sample was cleaved into 3 mm by 4mm pieces normal to the interfaces, using a diamond scriber. In order to create a cross-section, two of these pieces were glued face to face using M-Bond 610 adhesive, and baked on a hot plate at 150^{o}C for 2 hours. Silicon dummy mounts were then cut on a slow speed diamond saw in 3mm X 4mm sections and attached to the outside of each sandwich by gluing and baking for an additional hour. Specimen sandwiches were mounted on a glass slide with crystal bond and cut in 500μm thickness on the slow speed diamond saw. The resulting samples were glued onto quartz stubs (interface being parallel to the stub) and their thickness reduced to about 40μm using a Gatan disc grinder. The 40μm thick discs were then dimpled taking care to make the interface line at the contact area of the dimpling wheel.

This reduced the center of the specimen down to 5 - 15μm in preparation for the final stage of ion milling. Finally, the prepared samples were ion milled in a Gatan duomill from both sides at 11^{o} with a high-energy gun, and 10^{o} with the a low energy gun. This enables a large amount of area to become electron transparent. Cross-section samples were examined in a TOPCON EM002B microscope at 200KV (with C_s = 0.5mm and a resolution of 1.8Å).

3.8.4 Heat spreading characteristics:

We have used a small surface mount resistor of 75 ohms. It was glued onto the sample on the device side and a constant DC current of 74.7 mA was passed through the resistor for about 30 seconds. The intensity was measured for a point about 1-2mm away from the heater on a line parallel to the heater and is recorded as the software captures the images of the heating sample for every second. Four samples were used to determine these characteristics. These are (a) monitor or reference silicon with no coating on the back side, (b) silicon coated with AlN, (c) silicon coated with only diamond on the back side, and (d) silicon coated with both diamond and AlN on the back side.

The next chapter describes the results obtained while the discussion and interpretation of the results are discussed in Chapter 5.

Chapter 4

Results

The experimental details of all the deposition and characterization techniques used were described in detail in the previous chapter. The results of all characterization techniques that have been performed to test the integration of diamond heat spreaders into device processing in silicon are presented below.

The main drawbacks in integrating diamond heat spreaders into silicon technology are the possible diffusion of impurities during deposition of the films and oxidation of diamond above 600^{o}C in the presence of O_2 during the gate and field oxide growth and the dielectric oxide layer deposition. Hence, all characterization techniques have been aimed to test for the purity of the wafer after deposition of the composite thin film and to check for the stability of diamond. The samples used along with the characterization techniques were listed in table 1.2.

4.1 X-ray diffraction:

X-ray diffraction was performed on the samples to evaluate the crystallinity and the growth orientation of AlN on the Si (100) substrate (Si_3N_4 etched on the backside). Results of X-ray diffraction on the samples deposited with aluminum nitride by magnetron sputtering, and shown in fig.4.1, illustrate preferential growth of aluminum nitride on the (0002) basal plane. The silicon (400) and (200) peaks from the substrate also can be seen. The measured full width at half maximum (FWHM) of the AlN basal plane (0002) peak is 0.0052 radians.

4.2 Scanning electron microscopy (SEM):

The growth and morphology of diamond on AlN deposited on Si (100) (Si_3N_4 etched) is illustrated in fig.4.2.1. The triangular (111), and the rectangular (001) facets can be seen. Diamond is recognized by the presence of rectangular and triangular facets. There is a

high concentration of rectangular (001) facets. From the shape of these facets the favorable orientation and growth of the grains is seen to be cubic. It is also possible to map the elements found in an SEM image by X-ray analysis. The software with the instrument can scan the sample and create digital images or maps of each element. Thus, from the X-ray maps we can detect and determine distribution of different elements. The X-ray map of a similar region in the same sample is shown in figure 4.2.2 and illustrates the presence of the elements carbon, aluminum, nitrogen, oxygen and silicon. Figure 4.2.3 shows the presence of diamond after the oxidation step. Clusters of diamond called "cabbage diamond" can also be noticed. Excessive charging arising from the surface during this observation because of the presence of the protective insulating silicon nitride layer above diamond even at lower voltages, reduced the resolution. Figure 4.2.4 is the corresponding X-Ray map showing the presence of the elements carbon, nitrogen, oxygen, aluminum, and silicon.

4.3 Transmission electron microscopy (TEM):

The bright field images of the diamond and aluminum nitride interface are shown in figures 4.3.1 (a) and (b). The AlN grains can be observed in the low magnification image shown in fig. 4.3.1 (a). However, the grain boundaries in diamond are not seen in contrast at this low magnification. The interface between diamond and AlN is very non-uniform in thickness. Diamond grains can also be noticed in contrast in the high magnification image of the same region. The dark regions in the image correspond to precipitates and these may arise from graphite or other milling artifacts. Figures 4.3.2 (a) and (b) are the respective selective area diffraction patterns (SADP) of the interface region. AlN (112), (104), (213) reflections and the diamond (440), (311), and (111) reflections are observed.

Many unidentified reflections are also noticed. These could be associated with the precipitates on the surface. A more complete analysis of these reflections will be carried out.

4.4 Current-Voltage (I-V) characteristics:

I-V characteristics of a Schottky diode fabricated on the device side for the four sets of samples are shown in figures 4.4.1 and 4.4.2. The same Schottky barrier diodes were used subsequently for the deep level transient spectroscopy (DLTS) measurements. The samples used were, (a) reference Si without any films, (b) reference Si that had oxidation, (c) composite/Si(100) without oxidation, (d) composite/Si(100) that had oxidation. The I-V characteristics of the reference samples (a) and (b) listed above that did not have any thin film deposition are shown in fig.4.4.1. Also, the I-V characteristics of the samples (c) and (d) listed above are shown in fig.4.4.2. From these results, similar I-V characteristics are observed. All the samples have the same exponential behavior in the forward bias mode and the current values are almost zero in the reverse bias mode. All the diodes have a forward saturation current of 0.00997 amperes. The slope of the linear region in the logarithmic scale of I-V characteristics gives the ideality factor of the diode. The Schottky barrier height ϕ_b, calculated for the diode on the reference sample that had no films deposited is equal to 0.503eV and the ideality factor, n is equal to 6.116. Similar characteristics are seen in the reference sample oxidized at 1000^{o}C for 15 minutes. In this case, the Schottky barrier height ϕ_b, is equal to 0.504eV and the ideality factor, n is equal to 6.184. From the I-V characteristics of the composite coated samples that did not have the oxidation, the Schottky barrier height ϕ_b, is 0.528eV while the ideality factor is 6.018. The extracted Schottky barrier height and the ideality factor values for the composite

coated sample that had the same oxidation conditions as for the reference Si are 0.521eV and 14.94, respectively.

4.5 Deep level transient spectroscopy (DLTS):

Deep level transient spectroscopy (DLTS) has been performed on the substrates to determine the impurity levels generated in the wafer from the diamond deposition and/or also from the high temperature oxidation step. The DLTS spectra are compared between the reference silicon samples and the samples with AlN/diamond composite. The DLTS spectra for the reference silicon wafers, both oxidized and unoxidized are shown in figure 4.5.1. The spectra for the samples that had the composite coating of aluminum nitride followed by diamond is shown in figure 4.5.2. From the spectrum of the unoxidized reference Si sample, as shown in figure 4.5.1, only one peak of the Fe-B complex is seen at ~50K corresponding to a trap concentration of 8 x 10^{11} atoms/cm^3. Similarly, a trap concentration of 1.5 x 10^{12} atoms/cm^3 of the Fe-B complex is detected in the spectrum of the reference sample that underwent oxidation. Similar results are observed in DLTS in the samples that had the composite coating of aluminum nitride/diamond, as seen in figure 4.5.2. The Fe-B complex at ~ 50K has a trap concentration of 10^{11} atoms/cm^3. An Fe interstitial trap concentration of 8 x 10^{10} atoms/cm^3 is observed around 170K. No other peak except that corresponding to the Fe-B complex is seen in the spectrum shown in figure 4.5.2 of the oxidized sample with the composite aluminum nitride and diamond on the back. This peak corresponds to a trap concentration of 3 x 10^{12} atoms/cm^3.

4.6 Secondary ion mass spectroscopy (SIMS):

The SIMS results of analysis of C, O, N, and H in the three samples are shown in figures 4.6.1 to 4.6.3. The samples consist of (a) reference silicon sample that did not undergo

any thin film deposition, (b) composite coated Si, and (c) composite coated Si with oxidation treatment. In all the spectra, a shift in the depth profiles is the result of increase in the sputtering rate performed to overcome the background levels present in the chamber. Thus, the initial levels in all the spectra may be considered as background. Figure 4.6.1 shows the SIMS spectrum of the reference silicon giving the concentration of oxygen at 10^{18} atoms/cm^3, carbon at $1.5x10^{16}$ atom/cm^3, nitrogen at $5x10^{15}$ atoms/cm^3, and hydrogen at $1.5x10^{17}$ atoms/cm^3. Figure 4.6.2 is the SIMS spectrum of the sample with the composite AlN/diamond at the backside that did not have oxidation. In this case, the concentrations of carbon at $7x10^{15}$ atoms/cm^3, oxygen at $2x10^{17}$ atoms/cm^3, hydrogen at $4x10^{15}$ atoms/cm^3, and nitrogen at $2.5x10^{15}$ atoms/cm^3 have been found. However, it is also important to determine the concentrations of all the above elements after the high temperature step of the field oxide growth that is a part of device processing. The diffusion of carbon and other elements at higher temperatures encountered during oxidation may be responsible for generation of impurity and defect generated traps. The SIMS spectrum of the sample having the composite AlN/diamond at the backside with the field oxide grown on the device side is shown in figure 4.6.3. The concentrations of carbon at $7x10^{15}$ atoms/cm^3, oxygen at $8x10^{17}$ atoms/cm^3, hydrogen at $5x10^{16}$ atoms/cm^3, and nitrogen at $6x10^{15}$ are evaluated from the spectrum.

4.7 Heat spreading characteristics of the multilayer film:

The heat spreading characteristics of (a) reference Si that did not have any thin film deposition (b) Si coated with AlN only, (c) Si coated with diamond only, and (d) composite coated Si are illustrated in figure 4.7.1. The intensity measured by the IR camera is a direct measure of the temperature. The intensity is plotted with respect to

time in figure 4.7.1. Higher intensity implies higher temperature at the point on the wafer. A higher rise in temperature of the selected point on the sample for a given amount of time implies better heat spreading characteristics because, the localized heat from the surface mount resistor is transferred to the selected point. From the figure 4.7.1, it can be seen that the temperature rises linearly for the first two seconds after the current is passed through the resistor, and reaches equilibrium after the initial rise. The rise in the intensity in the first two seconds is a measure of the heat spreading capability of the substrate. The slope of the initial linear region is a direct measure of the increase in temperature of the selected point. The slope of the linear region for the composite coated Si sample is 117.5/sec. This is followed by a slope value of 96.18/sec in the case of Si sample coated only with diamond. In the sample coated only with the AlN, the value of the slope measured is 44/sec and for the reference silicon it is 36/sec.

Chapter 5

Discussion

5.1 X-ray diffraction:

Growth of hexagonal AlN is expected to be on the close packed or (0002) basal plane. The presence of only (0002) basal plane peak indicates that the growth is highly textured. Textured growth implies that all the grains are oriented in one direction that is the {0002}direction. Textured AlN film is a good diffusion barrier because all random oriented and large grain boundaries are eliminated. Because, diffusion through crystalline materials is dominated through grain boundaries, the reduction in grain boundaries reduces the possibility of diffusion of unwanted impurities, in this case carbon, oxygen, nitrogen, and other impurities in the processing gases. The full width at half maximum (FWHM) of the (0002) peak is an indication of the of the film crystalline quality and concentration of defects. A smaller value of FWHM indicates better crystallinity and less defects. The FWHM value of 0.0052 radians indicates a good crystalline nature of the film.

5.2 Scanning electron microscopy:

The facets of diamond seen in the image shown in figure 4.2.1 are an indication of the preferred growth orientation of diamond. It can be inferred that the growth is polycrystalline with majority of grains having (001) and a small number with (111) as the preferred orientations. Thus, cube textured growth of diamond is observed. The corresponding X-ray map in figure 4.2.2 indicates the presence of the elements carbon, oxygen, nitrogen, aluminum and silicon, and it is similar to the X-ray map of the sample that underwent oxidation as shown in figure 4.2.4. X-ray maps are not quantitative. Hence, only qualitative analysis has been performed by X-ray mapping. The uniform concentration of all the elements observed in the X-ray maps indicates no preferential

segregation in the heat spreaders. The concentration of oxygen is also very low. The presence of cabbage diamond as seen in fig.4.2.3 may have resulted from the preferential nucleation of diamond at certain regions in higher methane concentrations or lower temperature in certain regions of the large area samples. The plasma generated in the microwave plasma deposition system was sometimes uneven on the complete sample area. In particular, this was observed on large area samples and resulted in lower temperatures (<900^{o}C) and favorable growth conditions for cabbage diamond. The presence of diamond after the field oxide growth on the device side is a clear indication of the stability of the diamond during oxidation treatment. Thus, oxidation treatment of the device wafers does not cause the diamond film to be oxidized because of the silicon nitride protective layer.

5.3 Transmission electron microscopy:

An inter-reaction layer at the interface is seen in both the figures 4.3.1 (a) and (b). The presence of precipitates indicates that the interface is not defect free. The presence of a large interfacial region at the interface is not desirable because it increases the thermal resistance due to phonon scattering at these defects. A sharp diamond/AlN or a crystalline region with small thickness is desirable. The indexed diffraction spots in the SADP of the interface in figures 4.3.2 (a) and (b) indicate that the inter-reaction layer is a mixture of polycrystalline diamond and aluminum nitride. The unidentified reflections in the SADP may be coming from other reaction products between aluminum nitride and diamond. These reflections may also be arising from products formed from milling. Further analysis is being carried out to determine these reflections. Because a sharp interface or a crystalline interface with no amorphous pockets is desirable for low interfacial thermal

resistance, higher growth temperature of diamond with lower methane concentration is expected to be beneficial.

5.4 I-V characteristics of the Schottky diode:

The I-V characteristics of the reference samples from figure 4.4.1 can be used to interpret the characteristics of the samples with the integrated heat spreaders shown in figure 4.4.2. From both the figures, it can be inferred that all the diodes are rectifying with an exponential increase in current in the forward bias mode and almost zero current in the reverse bias mode. For an ideal Schottky diode, the ideality factor is one and the ideal Scottky barrier height for Ti on p-Si is 0.6eV. The standard deviation in the ϕ_b values of the samples is 0.012463 and indicates that there is no significant variation in the Schottky barrier height in the reference and the integrated heat spreaders. However, the ideality factor for the composite heat spreader that underwent oxidation is significantly higher than the other three. This deviation from ideality in all the cases is attributed to the reasons discussed earlier in section 2.5.1. The presence of a very thin native oxide may be the reason for the existence of interface states and the lowering of the barrier height.

Thus, the similar diode characteristics of reference silicon samples and the composite coated silicon samples strongly support device integration with diamond heat spreaders. The Schottky characteristics of integrated device samples similar to reference samples indicate the proper functioning of a device on the heat spreader samples. These results can be extended to the working of high-power devices also.

5.5 Deep level transient spectroscopy:

DLTS technique detects electrically active impurities and trap levels. From the DLTS, it is confirmed that there are no additional impurities introduced into the wafer because of the deposition of aluminum nitride and diamond on the backside. Also, no defects or impurities that could generate traps are formed during oxidation. The only electrically active impurity states seen in all the samples are the Fe-B complex and an Fe interstitial trap level noticed in the composite coated Si that did not undergo oxidation treatment. Thus, it can be concluded that the growth of aluminum nitride and diamond followed by the device integration including high temperature oxidation did not induce any electrically active impurities and did not affect the purity levels in the wafers as well as the Schottky device characteristics described earlier. These results support integration of AlN/diamond heat spreaders with device processing in silicon.

5.6 Secondary ion mass spectroscopy:

The SIMS spectra of the both the composite coated samples with and without oxidation illustrate that the concentrations of carbon, oxygen, nitrogen, and hydrogen are comparable to their levels in the reference silicon. Thus, further support is presented to show that there has been no contamination from diffusion of carbon and oxygen into the device side of the sample during aluminum nitride and diamond deposition. These results also show that no carbon, nitrogen or hydrogen diffused into the device side of the silicon during the high temperature oxidation as well. It can be concluded that integration of diamond heat spreaders into silicon device processing is possible without affecting the purity of the wafer.

5.7 Heat spreading characteristics:

From the figure 4.7.1, the AlN coated silicon shows an increase in intensity of 40 units while the reference silicon shows an increase by 30 units for the initial two seconds. The lower value in silicon is expected because the heat spreading characteristic depends on the thermal conducting films present on the back. The intensity is a direct measure of the temperature and it can be inferred from the slope values that the AlN coated silicon does not show significantly different rise in temperature although it is higher than that of reference Si. It can be concluded from this result that coating with AlN alone is not of significant advantage. Diamond coated Si sample shows an increase by 80 units while the composite coated silicon shows an increase of 130 units for the first two seconds. The slope value of the composite is the highest followed by diamond coated sample. Diamond with its unmatchable thermal conductivity must be the best heat spreader. However, as discussed earlier, continuous growth of diamond is not always achievable in CVD, especially in the initial stages. The presence of discontinuities like voids always reduces the effective thermal conductivity. The lower heat spreading capacity of diamond compared to the composite could be explained by the presence of defects such as voids in diamond. Also, thermal conductivity of diamond is a strong function of thickness and bulk values of thermal conductivity are achieved only when the thickness of the film is close to 200μm. The AlN layer beneath the diamond fills the voids that are present. Thus the AlN/diamond composite is undoubtedly a better heat spreader. These results also agree with previous results obtained on multilayer diamond heat spreaders deposited on high heat capacity substrate of molybdenum.

Chapter 6

Conclusions and future work

Conclusions

From the results of XRD, transmission and scanning electron microscopy, it has been shown that growth of high quality aluminum nitride and diamond can be achieved using the techniques of DC reactive magnetron sputtering, and microwave plasma enhanced CVD, respectively. The characterization results from DLTS showed that no electrically active impurities have been introduced into the wafers during the deposition of AlN and diamond. The SIMS results provide further support showing no increase in concentration of carbon, oxygen, nitrogen, and hydrogen in the heat spreader wafers when compared to the as received reference silicon wafers. The stability of diamond achieved by a thin silicon nitride diffusion barrier coating during the field oxide growth, as shown by SEM, further lends support to the conclusion that the integration of the heat spreaders into silicon device processing can be performed without oxidizing diamond. The heat spreading characteristics determined by infrared thermography, have illustrated the improved capability of using the composite AlN/diamond multilayer as an efficient heat spreader. Thus, by direct growth of the composite heat spreader on silicon, interfacial thermal resistances associated with bonding and the solder layers can be eliminated. Apart from this, the additional cost of bonding silicon wafer to diamond can be reduced and reliability of the heat spreaders and devices is improved. The lifetime of the heat spreader is also increased because the possibility of the solder failure due to frequent thermal cycling is eliminated. In summary, from all the results discussed, it has been conclusively shown that the purity of the wafers has not been affected by the deposition of aluminum nitride and diamond, high temperature stability of diamond in the presence of oxygen can be achieved, the composite has excellent heat spreader characteristics, and

therefore, the heat spreaders can be integrated into silicon device processing. The significance of successful integration of heat spreaders comes to fore especially in the case of high power and high frequency devices which constantly undergo thermal cycling because of the heat produced during their operation. Given the fact that the reliability costs in silicon technology because of thermal management run up to $200 billion annually, the results obtained are very significant for integration of diamond heat spreaders into silicon technology. Because the deposition techniques of DC RMS, and MPCVD are less expensive, easy to implement, and operate, the choice of a composite aluminum nitride/diamond heat spreader is definitely a cost effective alternative for spreading away the heat produced in the devices.

Future work

The results obtained in the present study are quite significant and nevertheless cannot be complete unless a more complete study of the interfaces in diamond/aluminum nitride, and diamond/silicon systems is performed. Because the interface thermal resistance is a drawback in the effective functioning of diamond as a heat spreader or heat sink, it should be minimized. Further improvement of the interface between AlN and diamond by reducing the thickness can lead to the development of highly efficient heat spreaders. A more extensive characterization of the defects like dislocations, voids, and presence of complex and amorphous phases at the interface by transmission electron microscopy and electron energy loss spectroscopy (EELS) will be helpful. A careful characterization on the presence of defects in the wafer is necessary because it has been observed very randomly that the samples coated with the composite are fragile and required careful handling throughout the experiments performed. Formation of brittle regions on the edge

of the samples by reaction of carbon with silicon could be one reason for the observed result. We have not provided extensive protection of the samples on the side of the samples. Also, protective silicon nitride film that is not etched away on the side may be responsible for the observed behavior. Defect free growth of diamond always improves the thermal conductivity of the diamond films because the phonon scattering at these defects is eliminated. Moreover, a highly oriented growth of diamond is preferable because the thermal conductivity of diamond is anisotropic and high in the (001) direction. The development of defect free and highly oriented growth of diamond can be a very significant contribution in the use of diamond as a very efficient heat sink material. Although, integration of AlN/diamond heat spreaders is investigated for processing Schottky devices and high temperature oxidation, treatments that cover a wide variety of device processing will be helpful to clarify any unforeseen processing conditions.

Figures and Tables

Properties of CVD diamond

Thermal conductivity In plane Perpendicular	 1400-1600W/m/K >2000W/m/K
Bandgap	5.5ev
Resistivity	10^{16} ohm-cm
Thermal expansion (RT-400^{o}C)	2.6 X 10^{-6}/^{o}C
Dielectric constant	5.6
Loss tangent	0.0005
Flexural strength	1000Mpa
Young's Modulus	1180Gpa
Density	3.51 gm/cm^{3}
Specific heat	0.54J/gm/K
Chemical resistance	All acids and alkalies

Table 1.1

Table 1.2

Characterization technique	**Samples prepared**	**Reason**
X-Ray diffraction.	AlN/Si(100) having Si_3N_4 on the device side.	To check for the growth orientation of AlN over Si.
Scanning electron microscopy (SEM).	(a) Composite* /Si(100) having Si_3N_4 on the device side. (b) Si_3N_4*/composite*/Si(100) that had oxidation treatment.	(a) To check for the morphology of the diamond surface after growth. (b) To check for the stability of diamond after oxide growth on the device side.
Transmission electron microscopy (TEM).	Cross section sample of diamond/AlN	To check for the interface characteristics of diamond/AlN.
I-V Schottky characteristics of a Schottky diode fabricated on the device side of the samples.	(a) Reference Si without any films. (b) Reference Si that had oxidation treatment. (c) Composite*/Si(100) without oxidation treatment. (d) Composite*/Si(100) that had oxidation treatment.	To check for the working of a diode built on the samples by comparing with reference Si and prove the integration of diamond heat spreaders.
Deep Level Transient Spectroscopy (DLTS).	(a) Reference Si without any films. (b) Reference Si that had oxidation treatment. (c) Composite*/Si(100) without oxidation treatment. (d) Composite*/Si(100) that had oxidation treatment	To detect electrically activities impurities if any in the samples after the deposition of the composite thin film coating by comparing with reference Si.
Secondary Ion Mass Spectroscopy (SIMS).	(a) Reference Si without any films. (b) Composite*/Si(100) without oxidation treatment. (c) Composite*/Si(100) that had oxidation treatment.	To check for the concentration of O_2, C in the samples after the composite thin film deposition by comparing with the reference Si.
Heat spreading characteristics.	(a) Reference Si without any films. (b) AlN/Si(100). (c) Diamond/Si. (d) Composite*/Si(100).	To test and compare the heat spreading characteristics of all the four samples listed.

Composite*: Refers to the multiplayer deposition of Diamond/AlN/Diamond.
Si_3N_4*: Refers to the presence of Si_3N_4 diffusion barrier layer over diamond.

Table 1.2

Properties of aluminum nitride

Thermal conductivity	140-180 W/m-K
Bandgap	6.2ev
Resistivity	10^{14} ohm-cm
Thermal expansion (RT-400^{o}C)	4.5 x 10^{-6}/^{o}C
Dielectric constant	9
Flexural strength	320Mpa
Young's Modulus	350Gpa
Density	3.26 gm/cm^{3}
Specific heat	0.74J/gm/K
Chemical resistance	Good, but etchable like other nitrides with a combination of HF/HNO_3.

Table 2.3.1

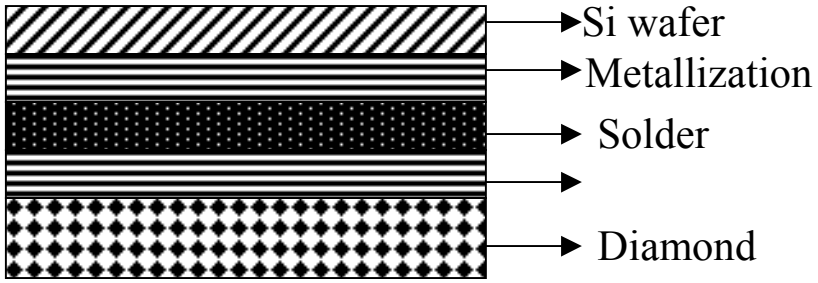
Si wafer
Metallization
Solder
Diamond

FIG.1.1

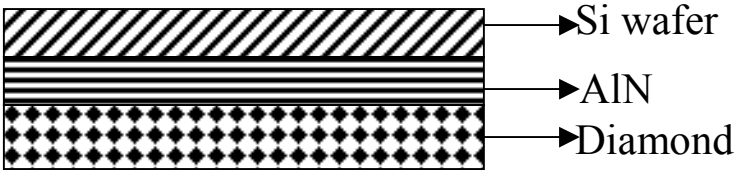
Si wafer
AlN
Diamond

FIG. 1.2

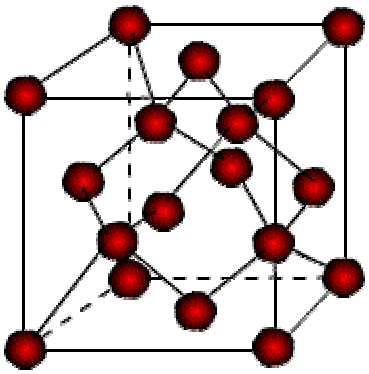

FIG. 2.1.1

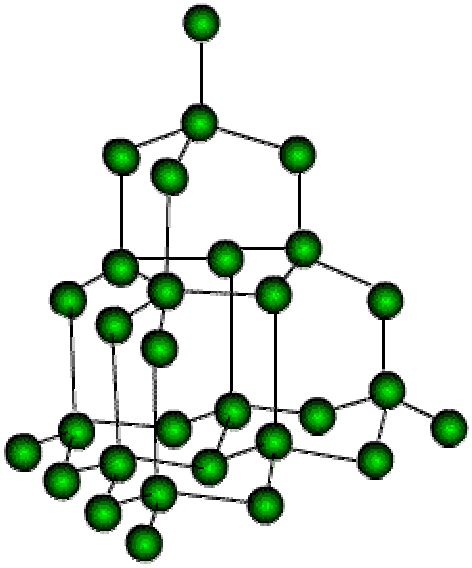

FIG. 2.1.2

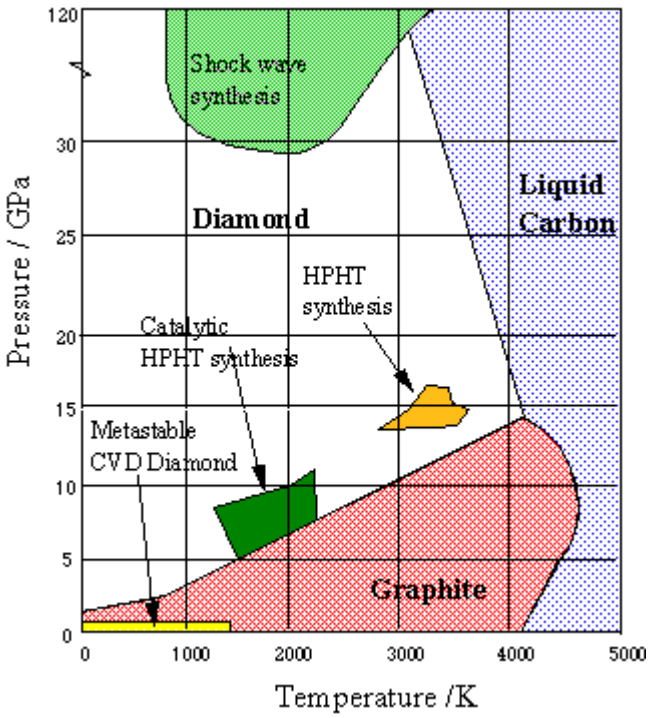

FIG. 2.2.1

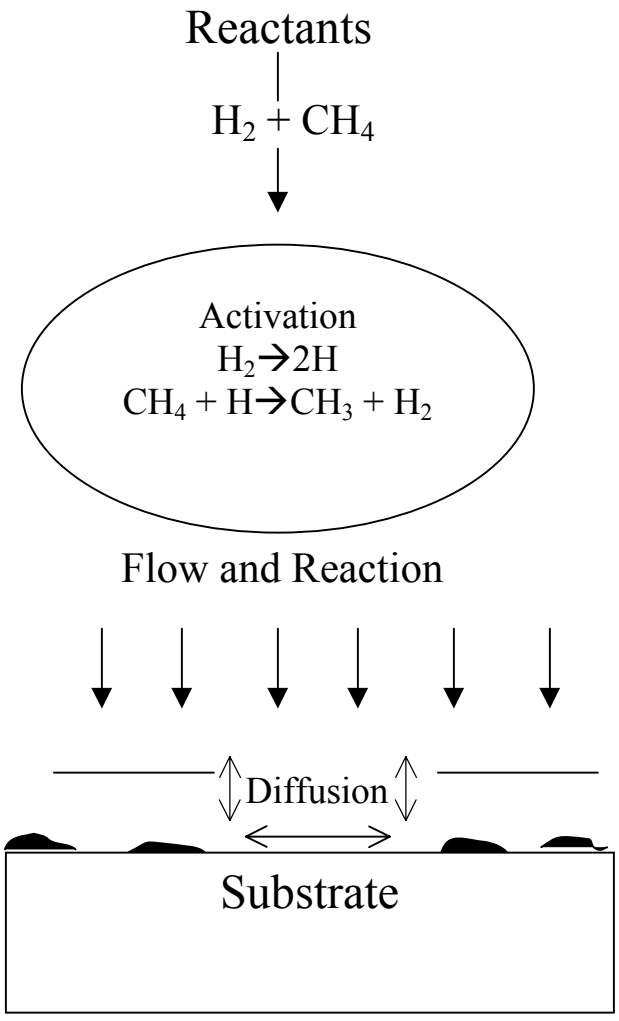
Reactants
$H_2 + CH_4$
Activation
$H_2 \rightarrow 2H$
$CH_4 + H \rightarrow CH_3 + H_2$
Flow and Reaction
Diffusion
Substrate

FIG. 2.2.2.1

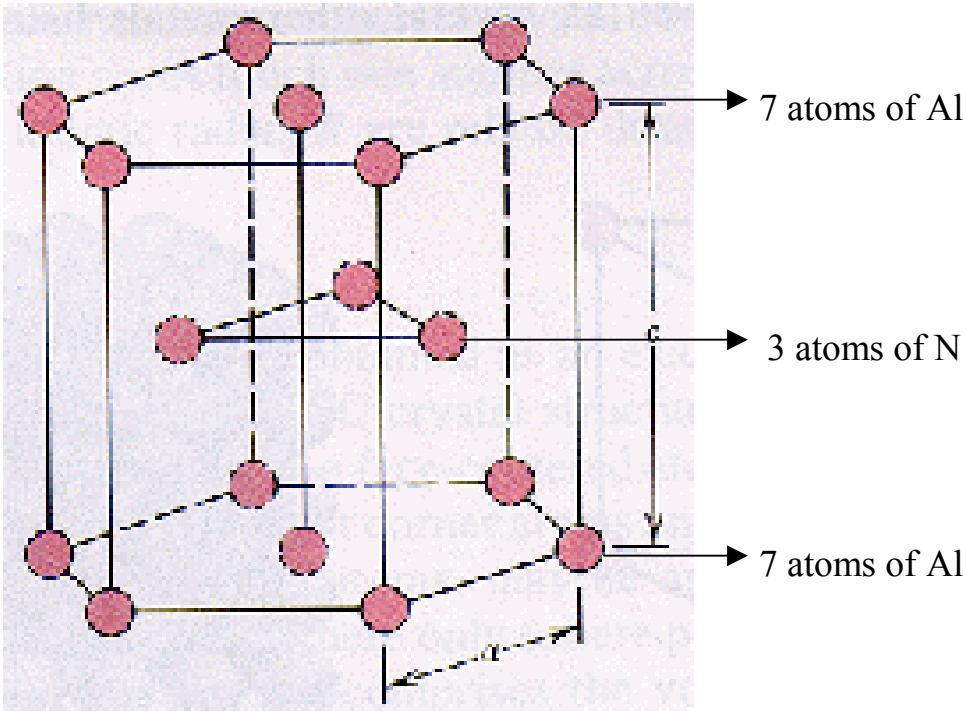

FIG. 2.3.1

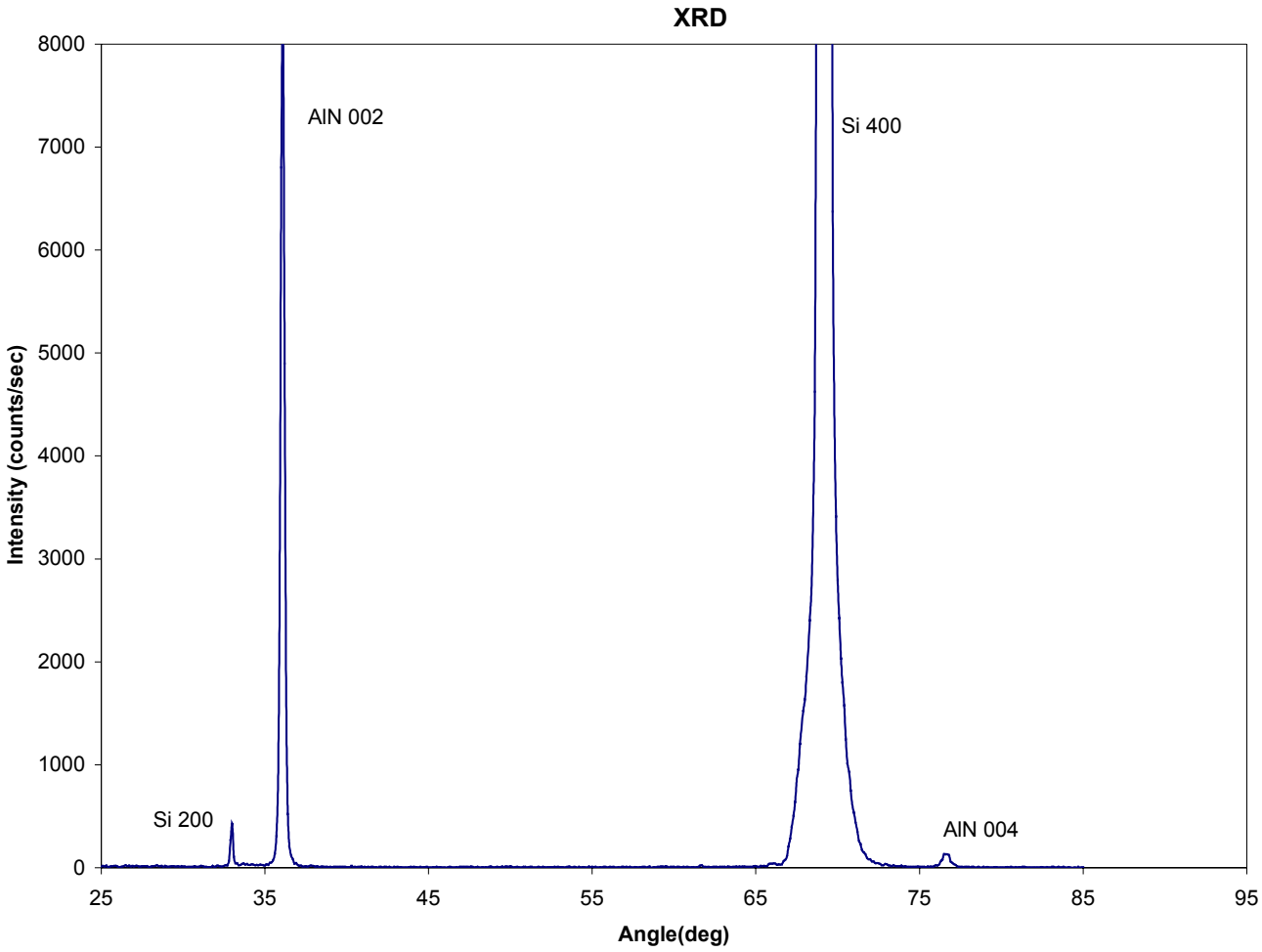
XRD
8000
7000
6000
5000
4000
3000
2000
1000
0
Intensity (counts/sec)
AlN 002
Si 400
Si 200
AlN 004
25
35
45
55
65
75
85
95
Angle(deg)

FIG 4.1.1

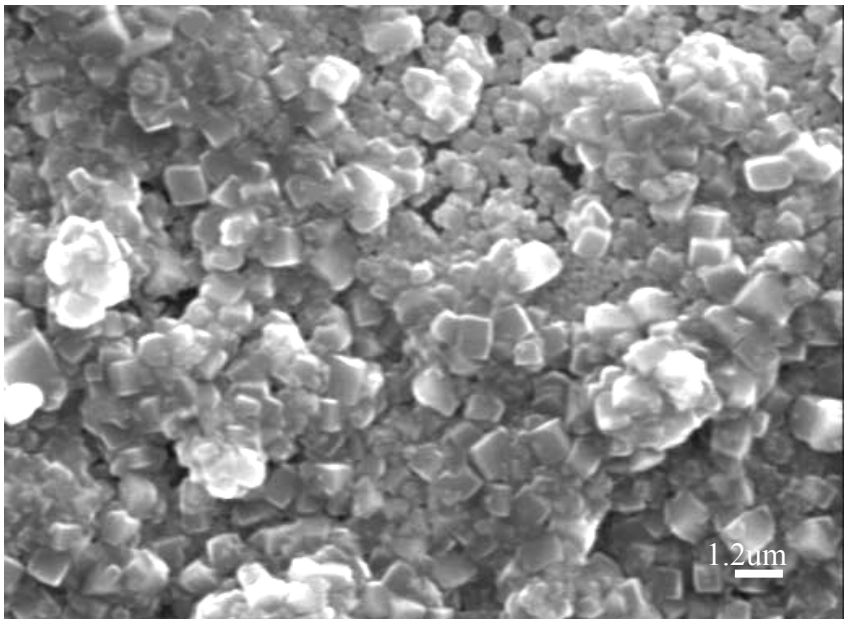

FIG 4.2.1

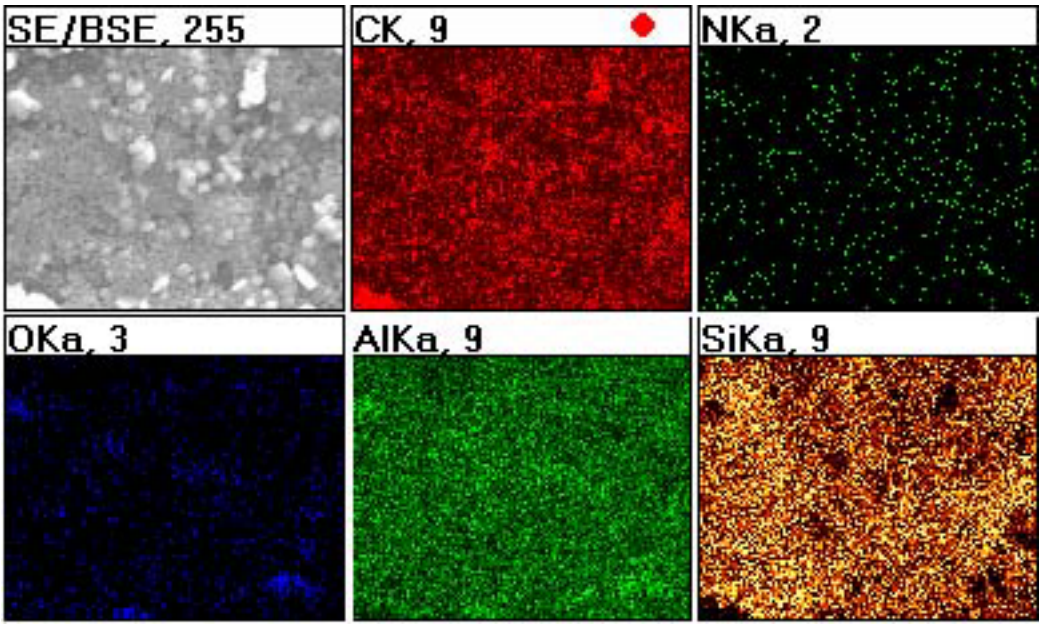

FIG 4.2.2

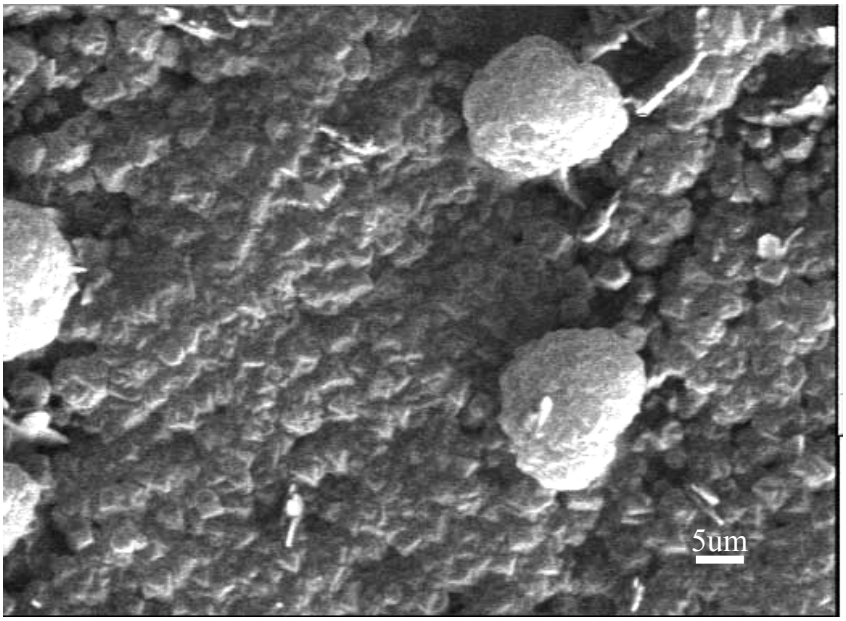

FIG 4.2.3

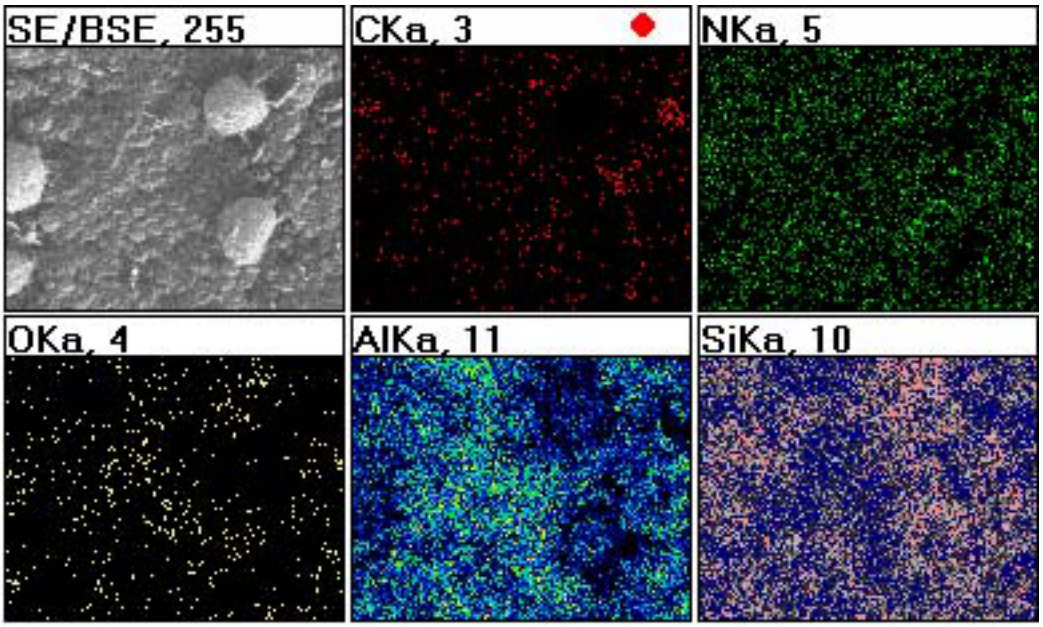

FIG 4.2.4

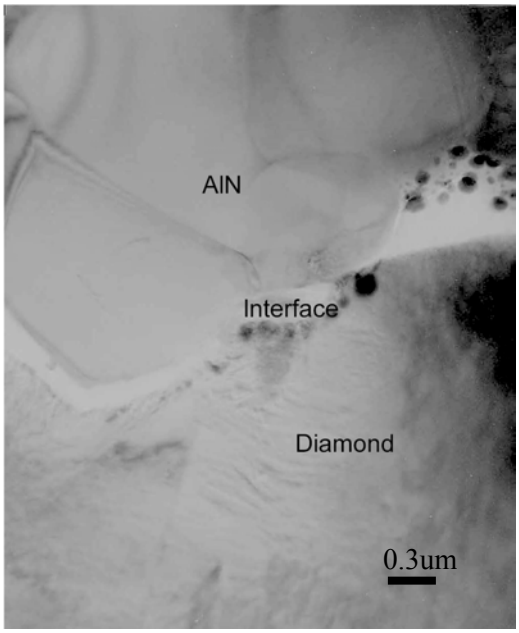

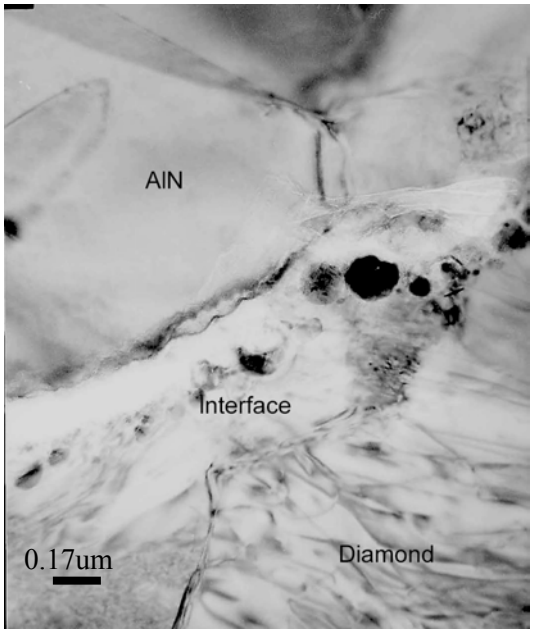

(a) (b)

FIG.4.3.1 (a) & (b)

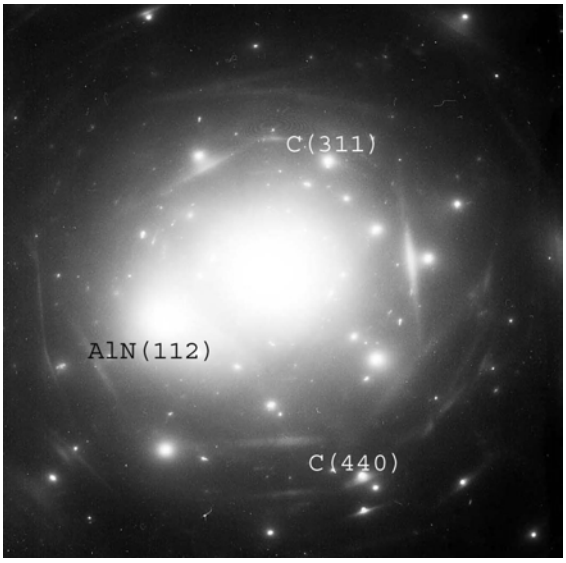

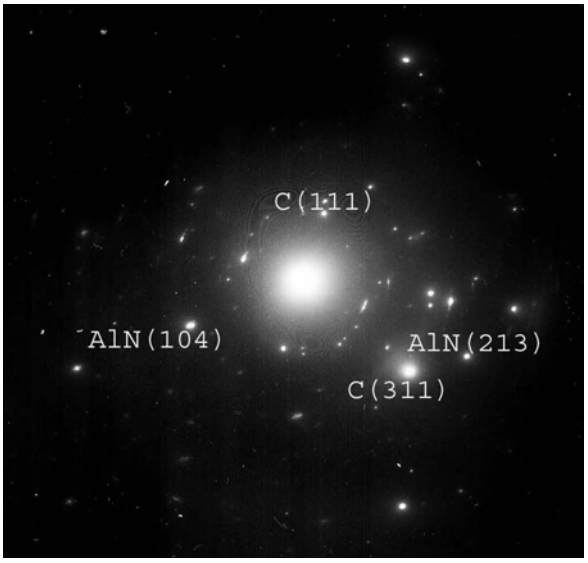

(a) (b)

FIG. 4.3.2 (a) & (b)

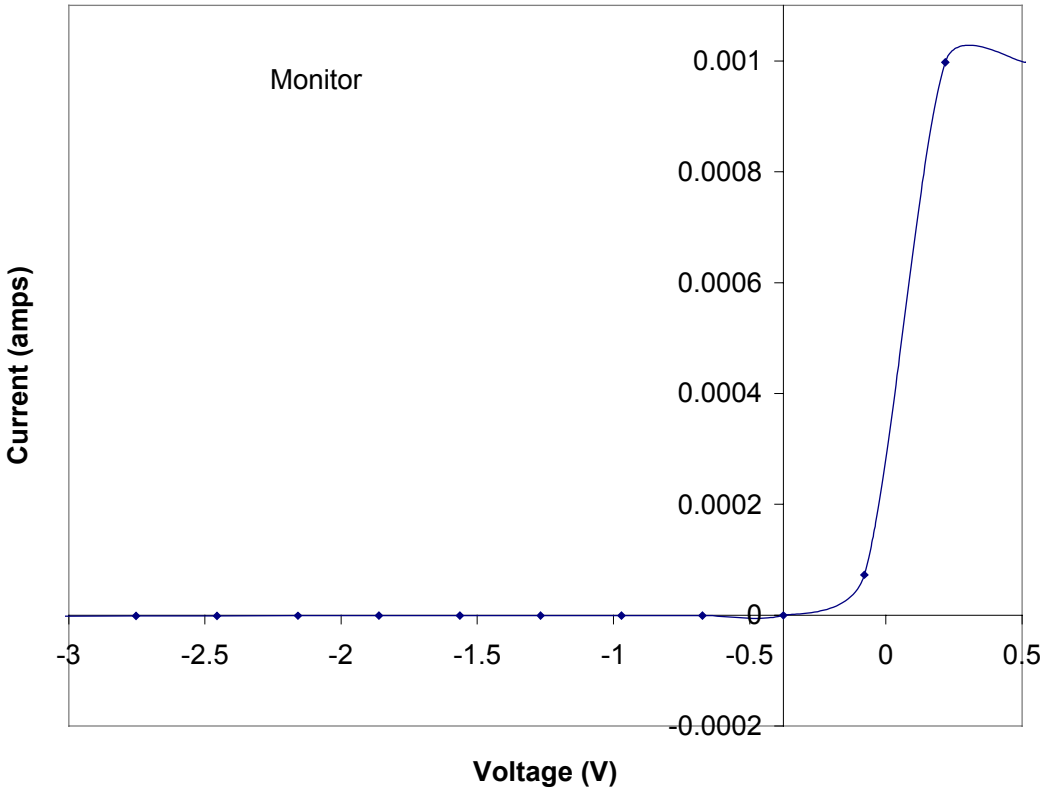
Monitor
Current (amps)
0.001
0.0008
0.0006
0.0004
0.0002
0
-0.0002
-3
-2.5
-2
-1.5
-1
-0.5
0
0.5
Voltage (V)

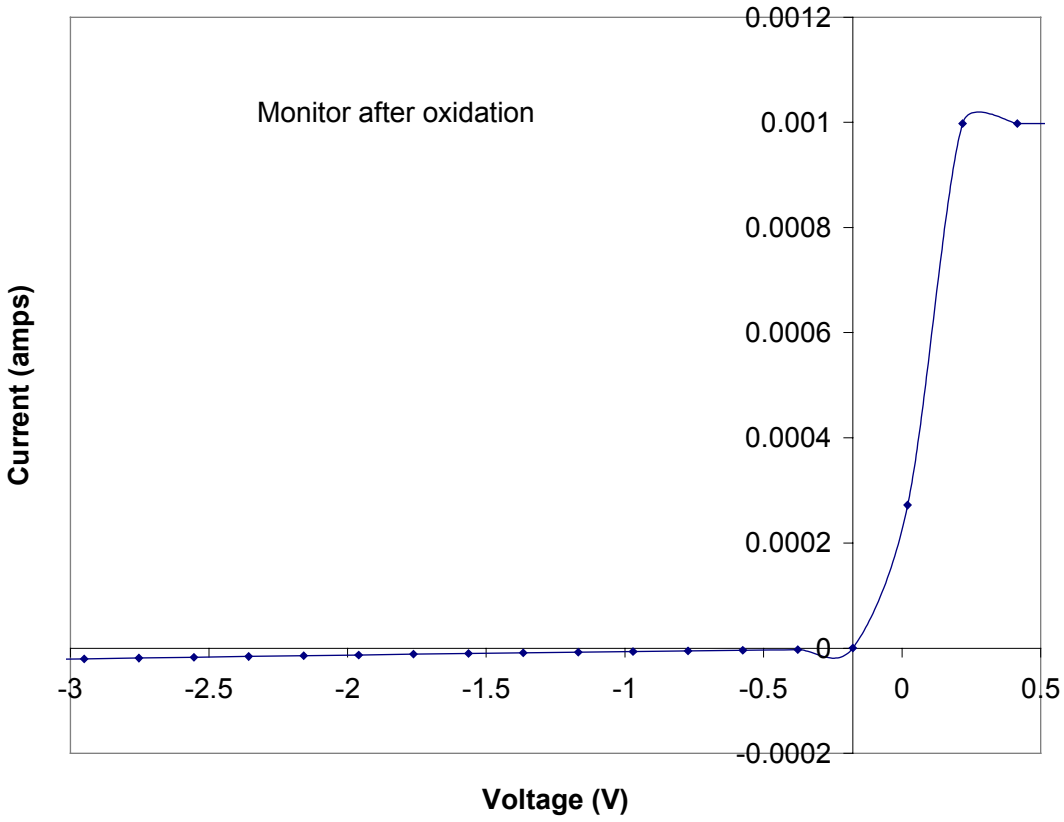
Monitor after oxidation
Current (amps)
0.0012
0.001
0.0008
0.0006
0.0004
0.0002
0
-0.0002
-3
-2.5
-2
-1.5
-1
-0.5
0
0.5
Voltage (V)

FIG. 4.4.1

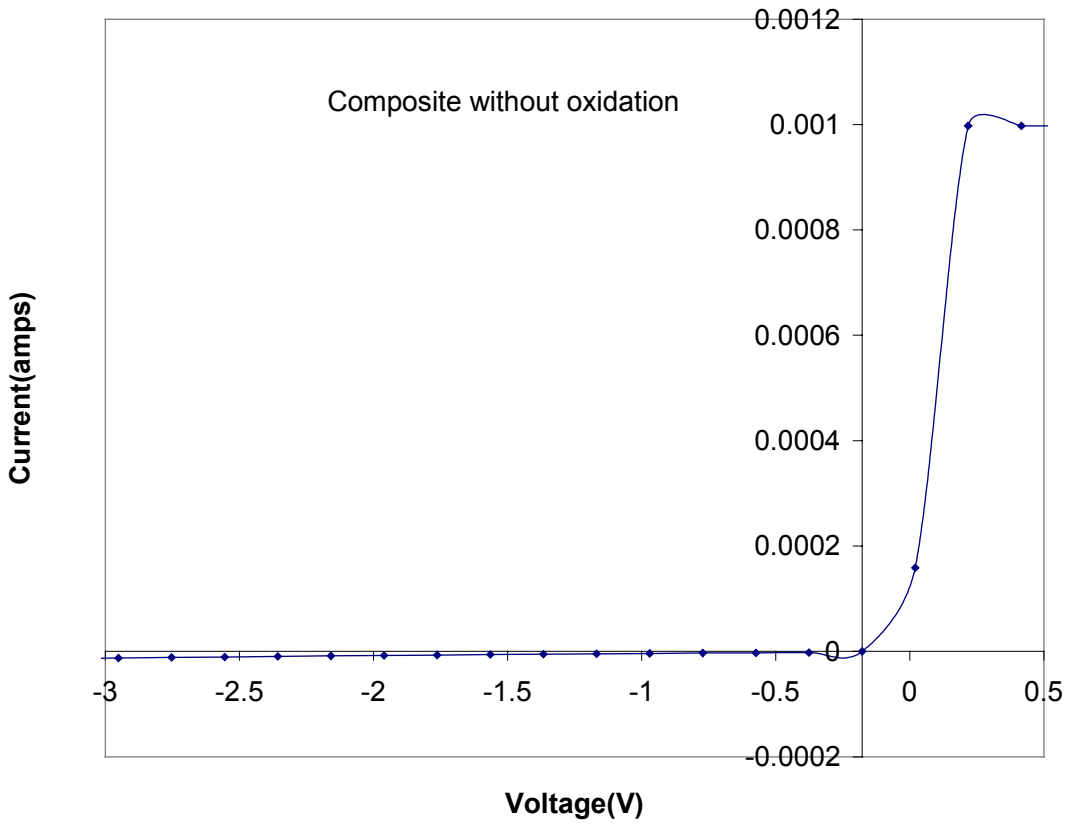
Composite without oxidation
Current(amps)
Voltage(V)
0.0012
0.001
0.0008
0.0006
0.0004
0.0002
0
-0.0002
-3
-2.5
-2
-1.5
-1
-0.5
0
0.5

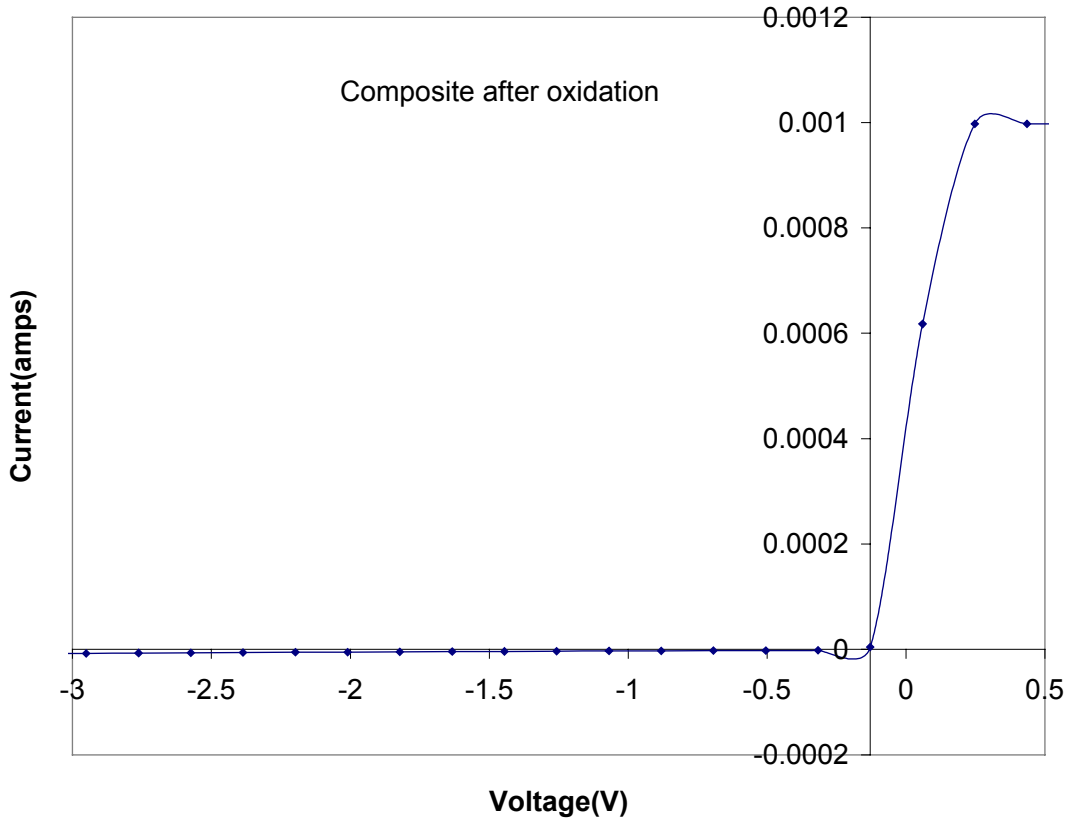
Composite after oxidation
Current(amps)
Voltage(V)
0.0012
0.001
0.0008
0.0006
0.0004
0.0002
0
-0.0002
-3
-2.5
-2
-1.5
-1
-0.5
0
0.5

FIG 4.4.2

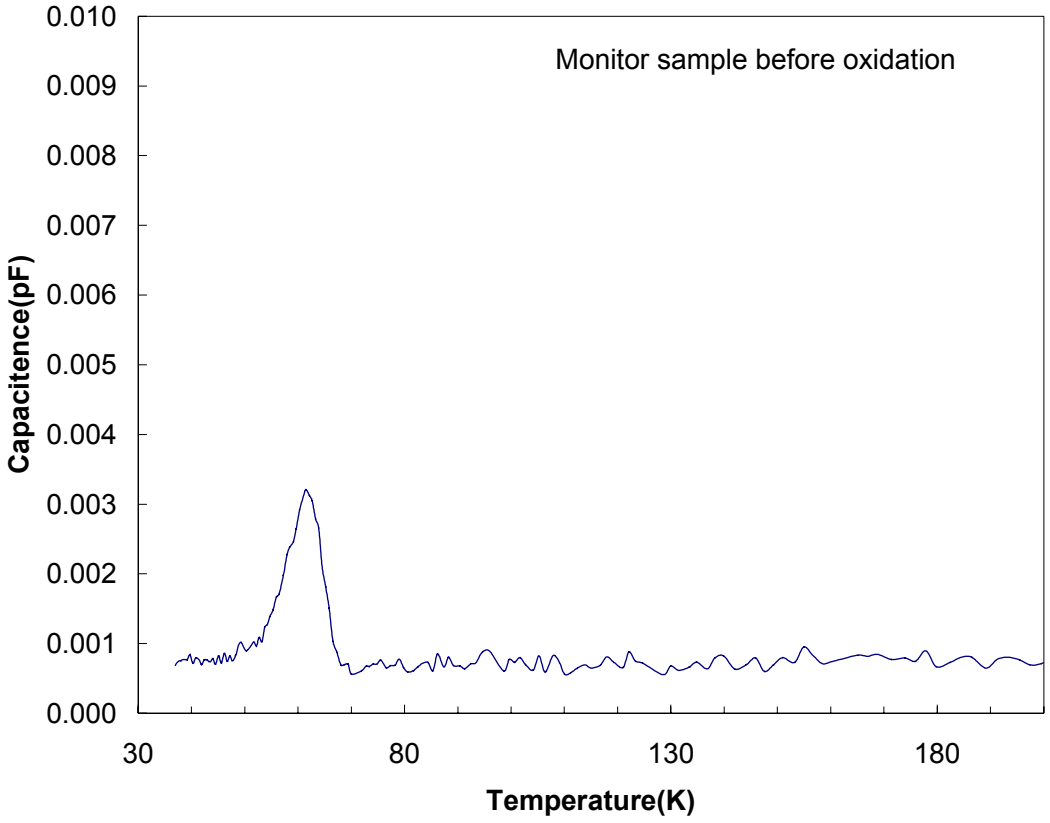
Monitor sample before oxidation
Capacitence(pF)
0.010
0.009
0.008
0.007
0.006
0.005
0.004
0.003
0.002
0.001
0.000
30
80
130
180
Temperature(K)

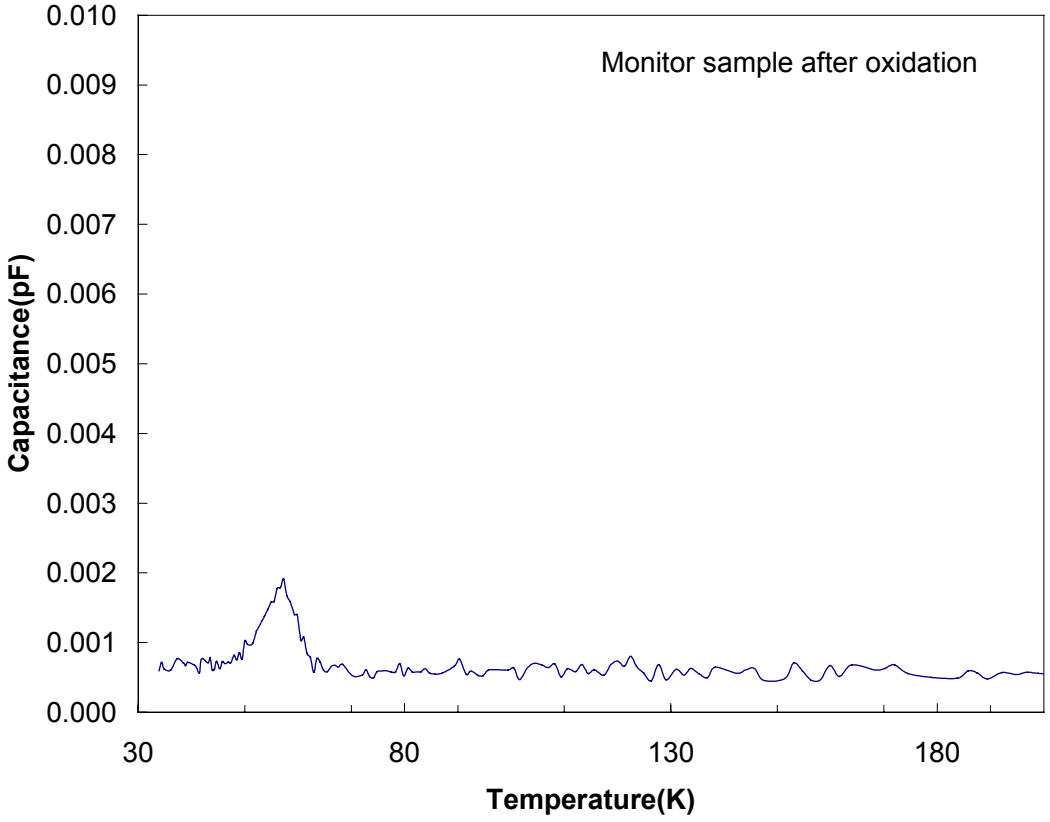
Monitor sample after oxidation
Capacitance(pF)
0.010
0.009
0.008
0.007
0.006
0.005
0.004
0.003
0.002
0.001
0.000
30
80
130
180
Temperature(K)

FIG 4.5.1

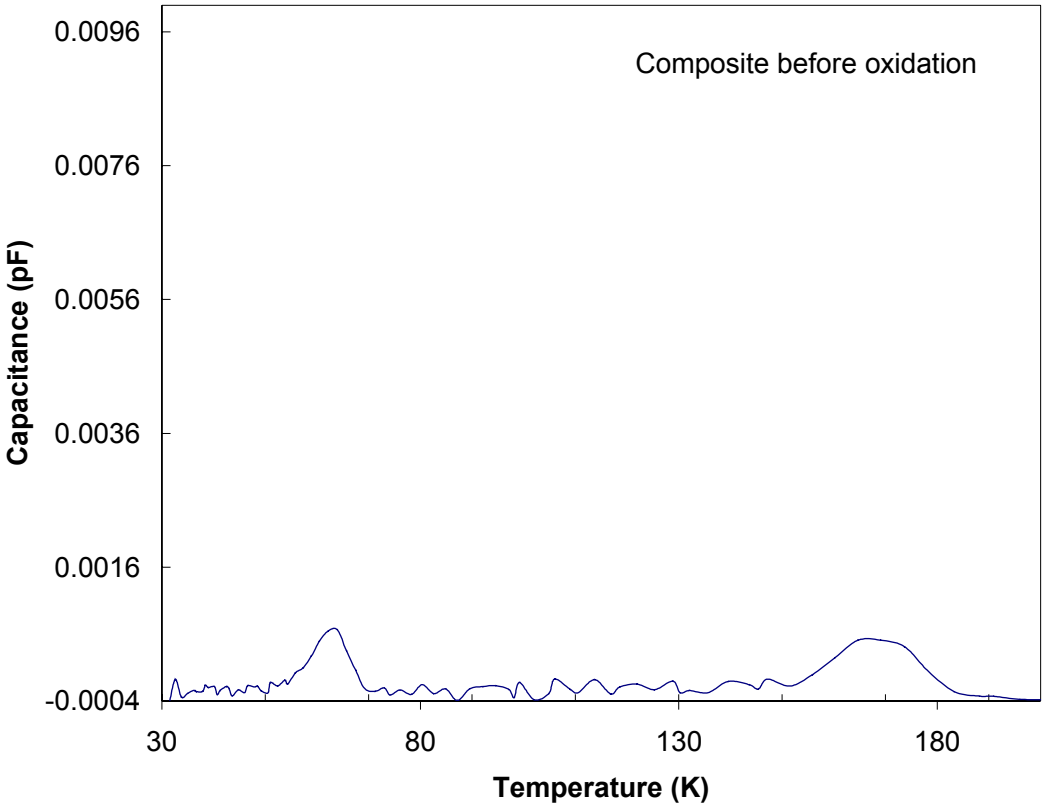
Composite before oxidation
0.0096
0.0076
0.0056
0.0036
0.0016
-0.0004
Capacitance (pF)
30
80
130
180
Temperature (K)

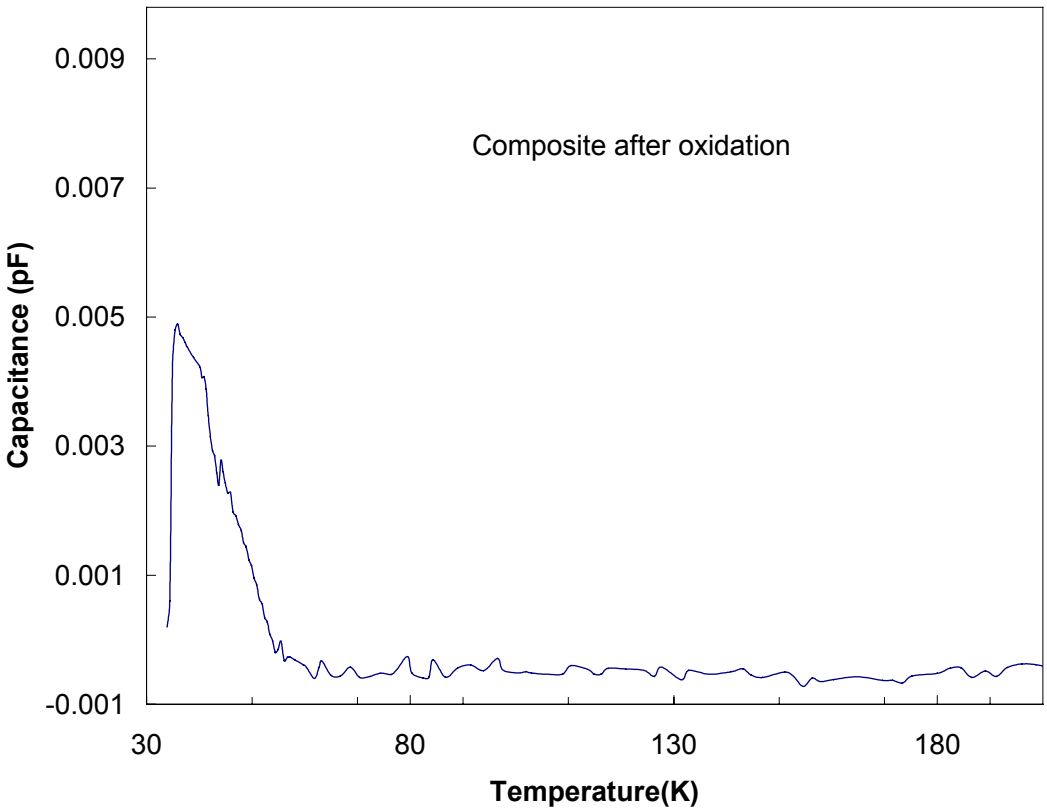
Composite after oxidation
0.009
0.007
0.005
0.003
0.001
-0.001
Capacitance (pF)
30
80
130
180
Temperature(K)

FIG 4.5.2

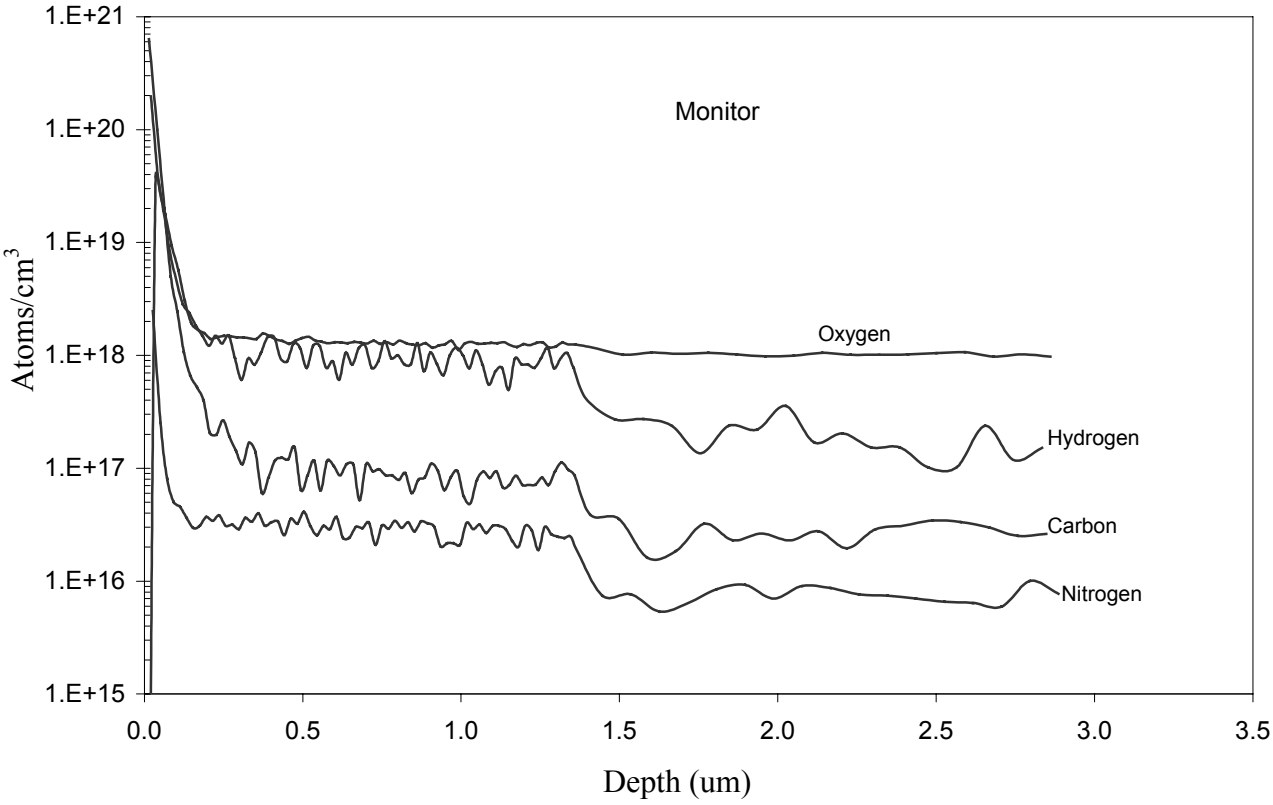
Monitor
Oxygen
Hydrogen
Carbon
Nitrogen
Atoms/cm3
1.E+21
1.E+20
1.E+19
1.E+18
1.E+17
1.E+16
1.E+15
0.0
0.5
1.0
1.5
2.0
2.5
3.0
3.5
Depth (um)

FIG. 4.6.1

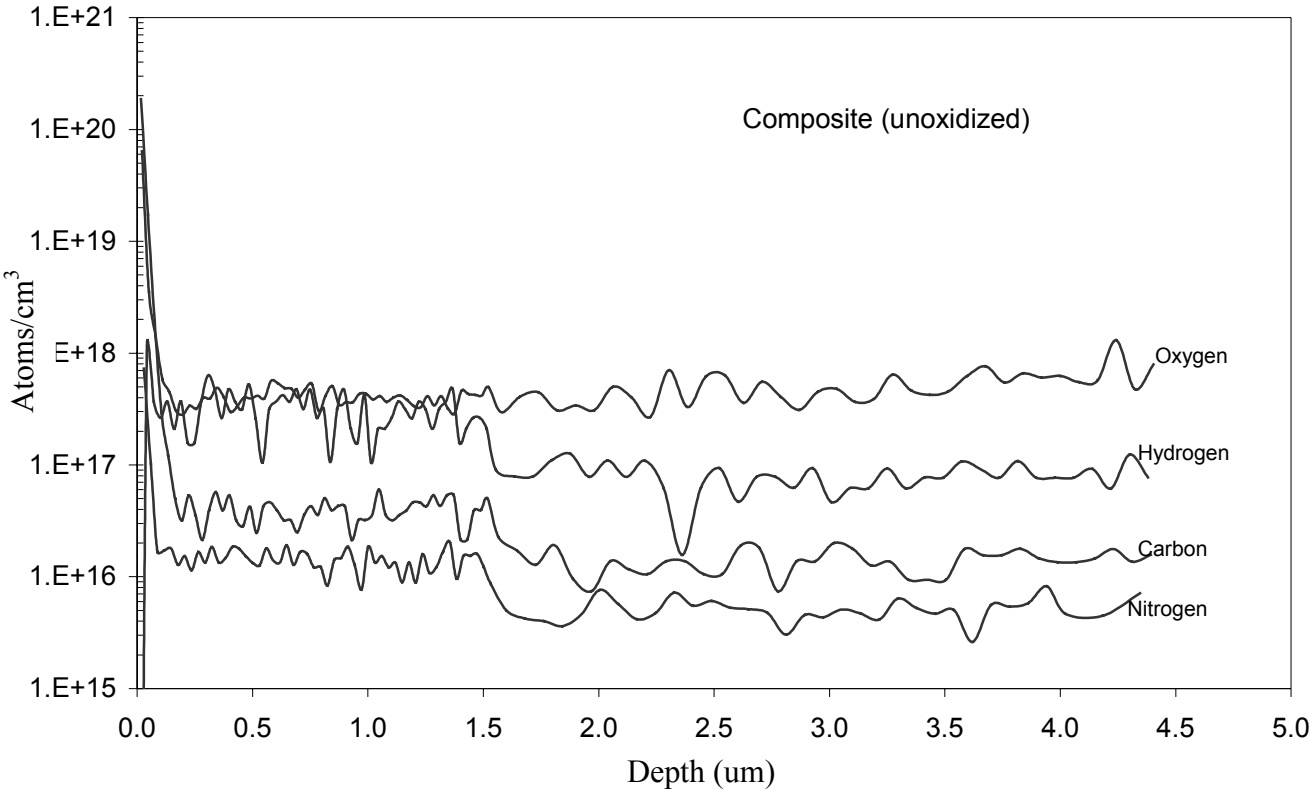
Composite (unoxidized)
Oxygen
Hydrogen
Carbon
Nitrogen
Atoms/cm3
Depth (um)
1.E+21
1.E+20
1.E+19
1.E+18
1.E+17
1.E+16
1.E+15
0.0
0.5
1.0
1.5
2.0
2.5
3.0
3.5
4.0
4.5
5.0

FIG. 4.6.2

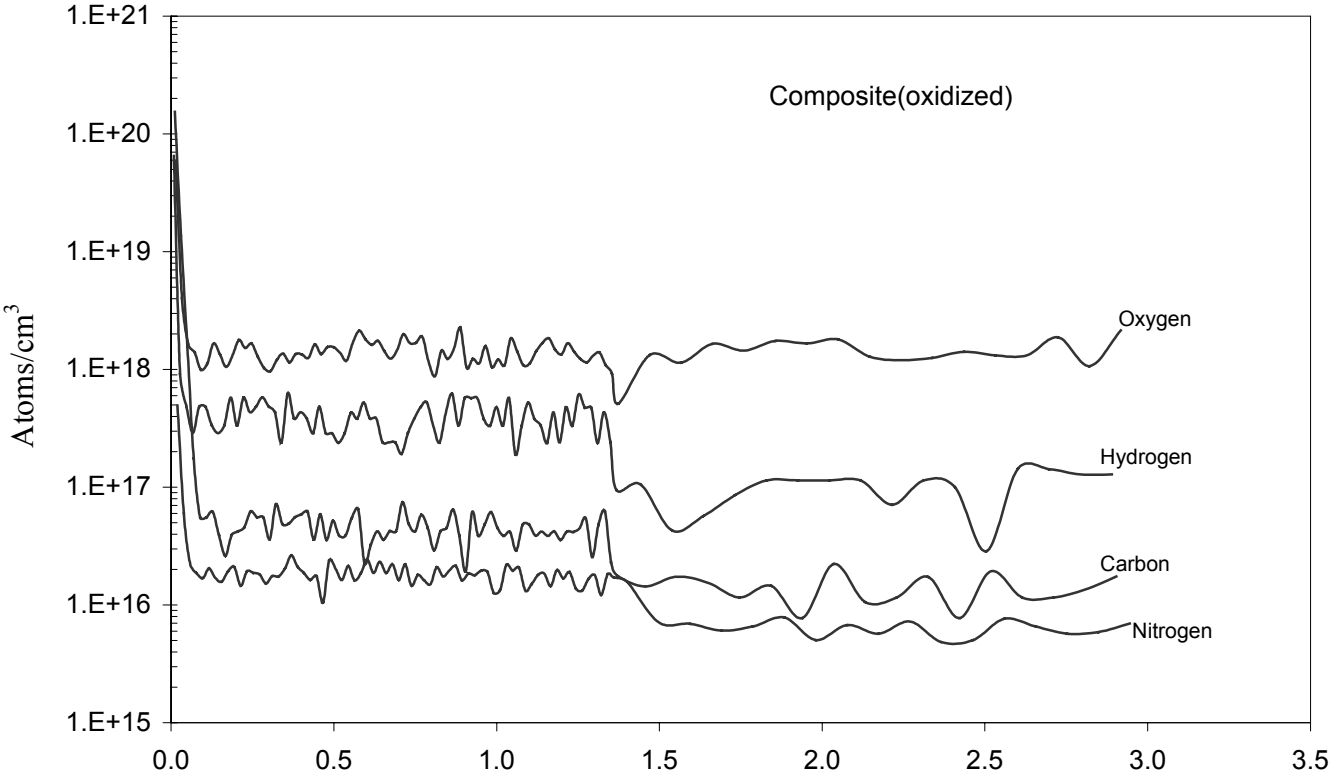
Composite(oxidized)
Atoms/cm3
1.E+21
1.E+20
1.E+19
1.E+18
1.E+17
1.E+16
1.E+15
0.0
0.5
1.0
1.5
2.0
2.5
3.0
3.5
Oxygen
Hydrogen
Carbon
Nitrogen

FIG. 4.6.3

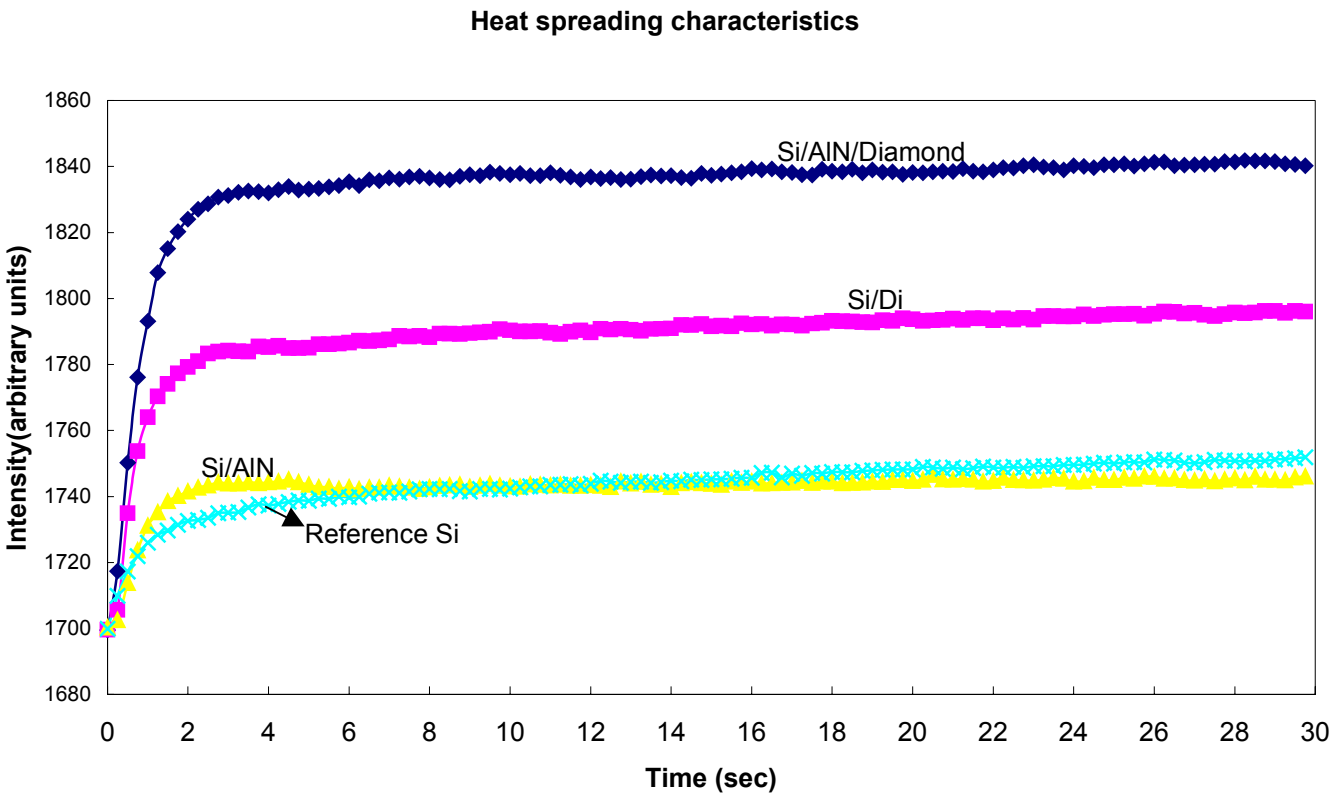
Heat spreading characteristics
Intensity(arbitrary units)
Time (sec)
Si/AlN/Diamond
Si/Di
Si/AlN
Reference Si
1860
1840
1820
1800
1780
1760
1740
1720
1700
1680
0
2
4
6
8
10
12
14
16
18
20
22
24
26
28
30

FIG.4.7.1

Appendix 1: Process flow

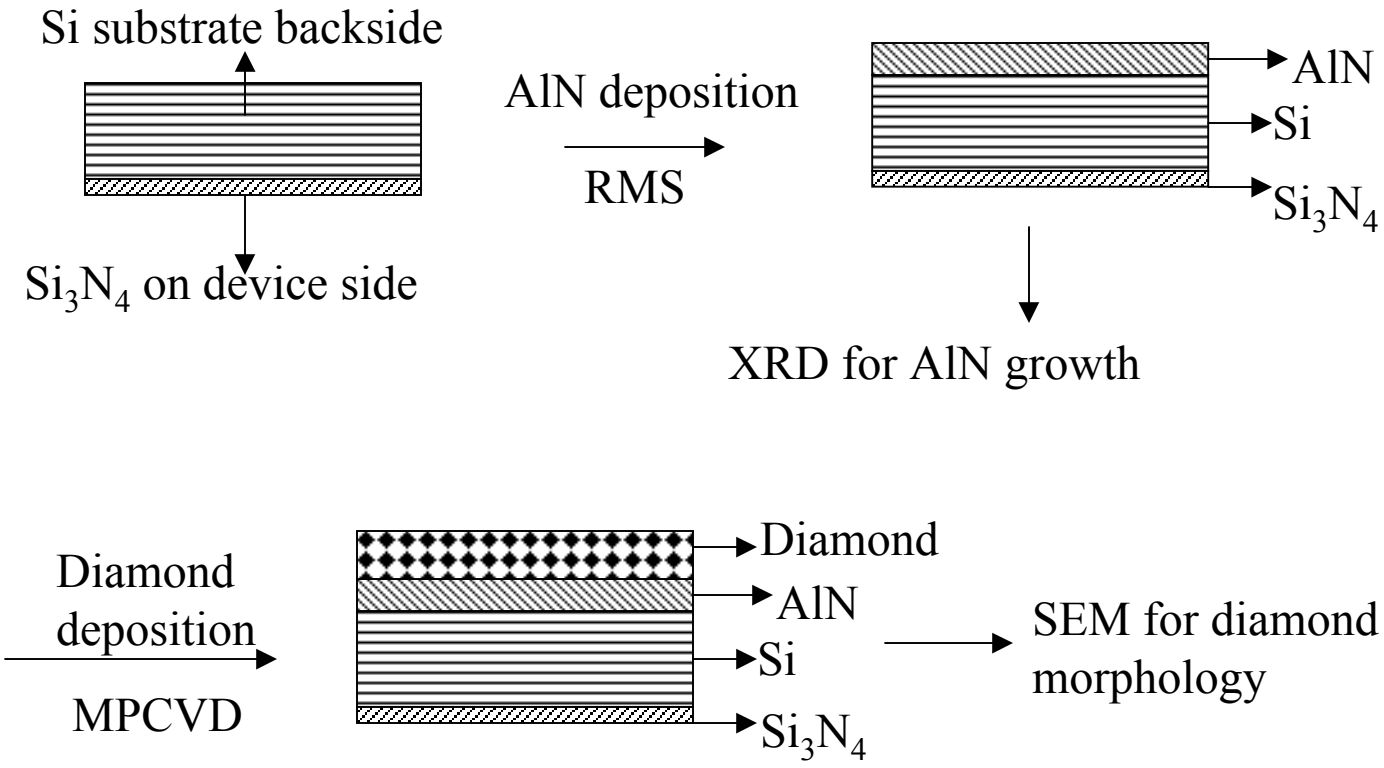

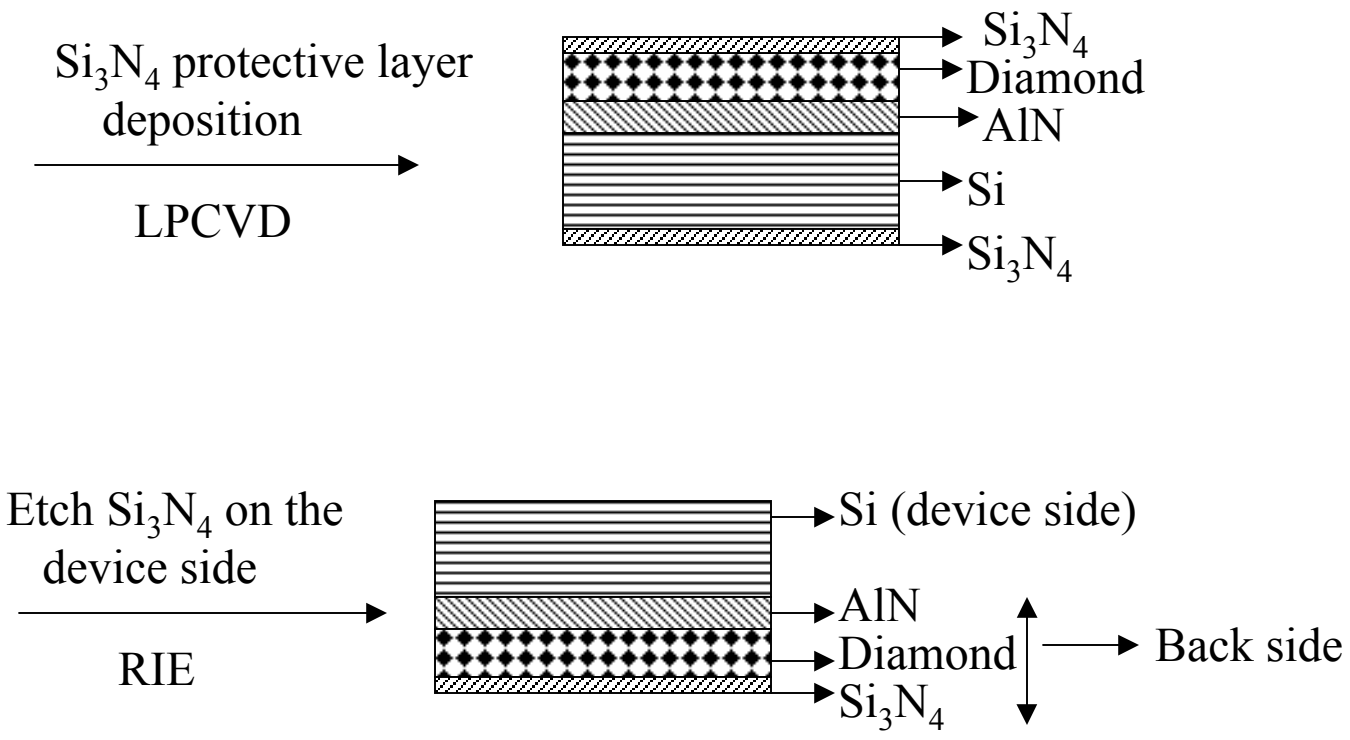
Si_3N_4 protective layer deposition
LPCVD
Si_3N_4
Diamond
AlN
Si
Si_3N_4
Etch Si_3N_4 on the device side
RIE
Si (device side)
AlN
Diamond
Si_3N_4
Back side

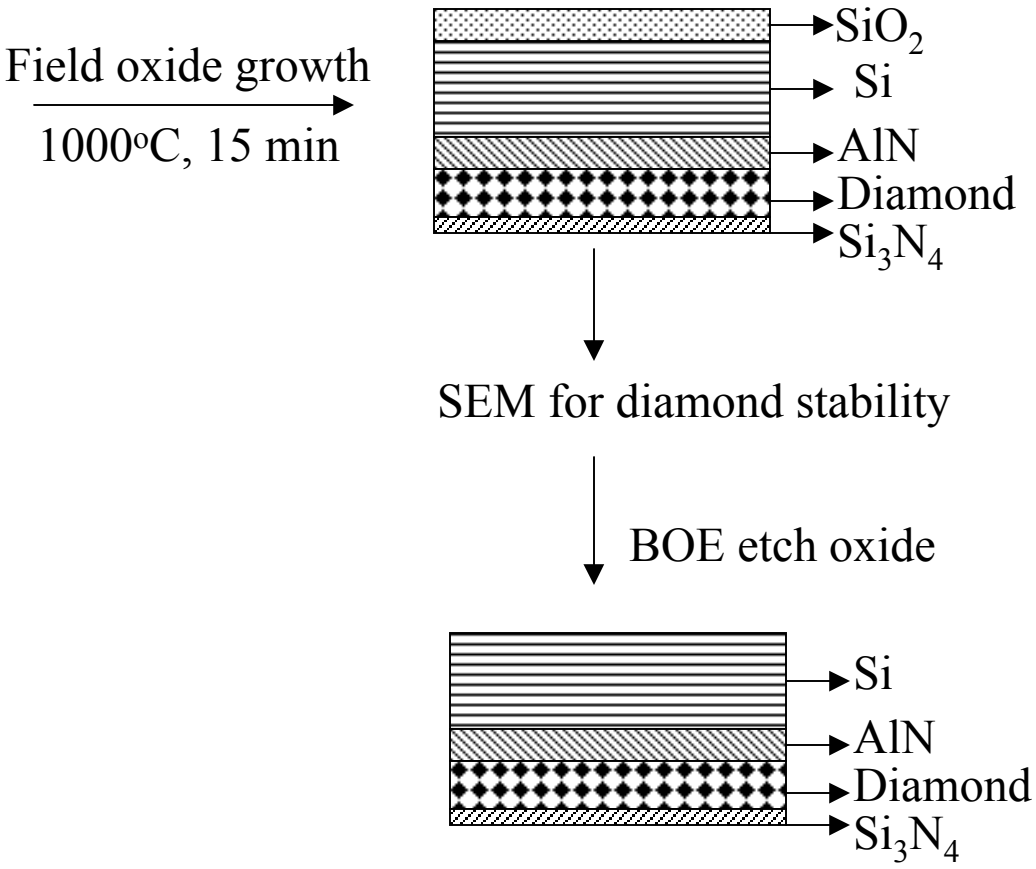
Field oxide growth
1000°C, 15 min
SiO2
Si
AlN
Diamond
Si3N4
SEM for diamond stability
BOE etch oxide
Si
AlN
Diamond
Si3N4

Ti-Al Schottky deposition

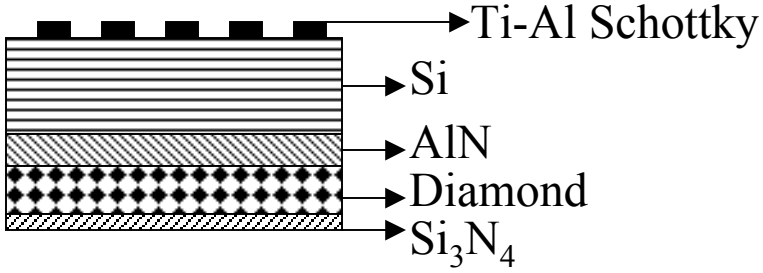

- Schottky characteristics for device integration
- DLTS and SIMS for impurity determination